EUROPEAN RESPIRATORY journal

FLAGSHIP SCIENTIFIC JOURNAL OF ERS

Early View

Original research article

Nasopharyngeal metatranscriptome profiles of infants with bronchiolitis and risk of childhood asthma: a multicentre prospective study

Yoshihiko Raita, Marcos Pérez-Losada, Robert J. Freishtat, Andrea Hahn, Eduardo Castro-Nallar, Ignacio Ramos-Tapia, Nathaniel Stearrett, Yury A. Bochkov, James E. Gern, Jonathan M. Mansbach, Zhaozhong Zhu, Carlos A. Camargo, Kohei Hasegawa

Please cite this article as: Raita Y, Pérez-Losada M, Freishtat RJ, *et al*. Nasopharyngeal metatranscriptome profiles of infants with bronchiolitis and risk of childhood asthma: a multicentre prospective study. *Eur Respir J* 2021; in press (https://doi.org/10.1183/13993003.02293-2021).

Nasopharyngeal metatranscriptome profiles of infants with bronchiolitis and risk of childhood asthma: a multicentre prospective study

Authors: Yoshihiko Raita, MD, MPH, MMSc[1*]; Marcos Pérez-Losada, PhD[2,3]; Robert J. Freishtat, MD, MPH[4,5,6]; Andrea Hahn, MD, MS[4,6,7]; Eduardo Castro-Nallar, PhD[8]; Ignacio Ramos-Tapia, PhD[8]; Nathaniel Stearrett[9]; Yury A. Bochkov, PhD[10]; James E. Gern, MD[10,11]; Jonathan M. Mansbach, MD, MPH[12]; Zhaozhong Zhu, ScD[1]; Carlos A. Camargo, Jr., MD, DrPH[1]; and Kohei Hasegawa, MD, MPH, MS[1]

Affiliations:

1. Department of Emergency Medicine, Massachusetts General Hospital, Harvard Medical School, Boston, MA, USA
2. Computational Biology Institute, Department of Biostatistics and Bioinformatics, The George Washington University, Washington, DC, USA
3. CIBIO-InBIO, Centro de Investigação em Biodiversidade e Recursos Genéticos, Universidade do Porto, Campus Agrário de Vairão, Vairão, Portugal
4. Center for Genetic Medicine Research, Children's National Research Institute, Washington, DC, USA

5. Division of Emergency Medicine, Children's National Hospital, Washington, DC, USA
6. Department of Pediatrics, George Washington University School of Medicine and Health Sciences, Washington, DC, USA
7. Division of Infectious Diseases, Children's National Hospital, Washington, DC, USA
8. Centro de Bioinformática y Biología Integrativa, Universidad Andres Bello, Avenida República 330, Santiago, Chile
9. Computational Biology Institute, George Washington University, Washington, DC, USA
10. Department of Pediatrics, University of Wisconsin School of Medicine and Public Health, Madison, Wisconsin, USA
11. Department of Medicine, University of Wisconsin School of Medicine and Public Health, Madison, Wisconsin, USA
12. Department of Pediatrics, Boston Children's Hospital, Harvard Medical School, Boston, MA, USA

Corresponding Author: Dr Yoshihiko Raita, Department of Emergency Medicine, Massachusetts General Hospital, 125 Nashua Street, Suite 920, Boston, MA 02114-1101. Tel: 617-726-5276, FAX: 617-724-4050.

E-mail: yraita1@alumni.jh.edu

Take Home Message: Our data suggest a complex interplay between the respiratory virus, airway microbiome, and host immune response in infants with severe bronchiolitis, and their integrated contributions to the subsequent development of childhood asthma.

Conflicts of Interest Statement: Dr. Bochkov has patents on production methods of rhinoviruses. Dr. Gern is a paid consultant to AstraZeneca and Meissa Vaccines Inc., has stock options in Meissa Vaccines Inc., and has patents on production methods of rhinoviruses. The other authors have no financial relationships relevant to this article to disclose.

Twitter feed comments: Metatranscriptome profiles identified by clustering analysis suggest a complex interplay between the respiratory virus, airway microbiome, and host immune response in infants with severe bronchiolitis, and their integrated contributions to the subsequent risk of childhood asthma.

ABSTRACT

The question addressed by the study

Bronchiolitis is not only the leading cause of hospitalization in U.S. infants but also a major risk factor for asthma development. Growing evidence supports clinical heterogeneity within bronchiolitis. To identify metatranscriptome profiles of infant bronchiolitis, and examine their relationship with host transcriptome and subsequent asthma development.

Materials/patients and methods

As part of multicentre prospective cohort study of infants (age <12 months) hospitalized for bronchiolitis, we integrated virus and nasopharyngeal metatranscriptome (species-level taxonomy and function) data measured at hospitalization. We applied network-based clustering approaches to identify metatranscriptome profiles. We then examined their association with host transcriptome at hospitalization and risk for developing asthma.

Results

We identified five metatranscriptome profiles of bronchiolitis (n=244):

A) virus^{RSV}microbiome^{commensals}, B) virus$^{RSV/RV\text{-}A}$microbiome$^{\textit{H.influenzae}}$,

C) virus^{RSV}microbiome$^{\textit{S.pneumoniae}}$, D) virus^{RSV}microbiome$^{\textit{M.nonliquefaciens}}$, and

E) virus$^{RSV/RV\text{-}C}$microbiome$^{\textit{M.catarrhalis}}$. Compared with profile A, profile B infants were characterized by high proportion of eczema, *H. influenzae* abundance, and enriched virulence

related to antibiotic resistance. These profile B infants also had upregulated T_H17 and downregulated type I interferon pathways (FDR<0.005) and significantly higher risk for developing asthma (17.9% vs. 38.9%; adjOR, 2.81; 95%CI, 1.11–7.26). Likewise, profile C infants were characterized by high proportion of parental asthma, *S. pneumoniae* dominance, and enriched glycerolipid and glycerophospholipid metabolism of microbiome. These profile C infants had upregulated receptor for advanced glycation end products signalling pathway (FDR<0.005) and higher risk of asthma (17.9% vs. 35.6%; adjOR, 2.49; 95%CI, 1.10–5.87).

Answer to the question

Metatranscriptome and clustering analysis identified biologically-distinct metatranscriptome profiles that have differential risks of asthma.

INTRODUCTION

Bronchiolitis is the leading cause of hospitalization in U.S. infants, accounting for ~110,000 hospitalizations annually [1]. In addition to the substantial acute morbidity, ~30% of infants hospitalized for bronchiolitis ("severe bronchiolitis") subsequently develop asthma [2]. However, the underlying mechanisms linking these two common conditions remain unclear. This major knowledge gap has hindered efforts to prevent asthma in this high-risk population.

Although bronchiolitis has traditionally been thought of as a single disease entity [3], growing evidence supports heterogeneity in the clinical manifestations [4] and pathobiology (e.g., as reflected by between-virus differences in the upper airway microbiome [via 16S rRNA gene sequencing]) [5–7]. Additionally, studies also suggest a complex interplay between viruses, microbiome, and host response in the airway, and its interrelationship with respiratory health [2, 8–14]. Despite the clinical and research significance, no study has integrated virus and airway microbiome (both taxonomy and function) data to investigate the metatranscriptome profiles of bronchiolitis, their relationship with the host response during the critical period of airway development (i.e., early infancy), and their contribution to incident asthma in later childhood.

To address this knowledge gap, we analysed data from a multicentre prospective cohort to 1) identify nasopharyngeal metatranscriptome profiles (or clusters) of bronchiolitis, and 2) investigate their association with host airway response and subsequent development of asthma.

METHODS

Study Design, Setting, and Participants

We analysed data from a multicentre prospective cohort study of infants hospitalized for bronchiolitis—the 35th Multicenter Airway Research Collaboration (MARC-35) study. Details of the study design, setting, participants, data collection, testing, and statistical analysis may be found in the **Supplementary Methods** of the **Supplementary Materials**.

Briefly, at 17 sites across 14 U.S. states (**Supplementary Table S1**), MARC-35 enrolled infants (age <1 year) who were hospitalized with an attending physician diagnosis of bronchiolitis during three bronchiolitis seasons in 2011-2014. The diagnosis of bronchiolitis was made according to the American Academy of Pediatrics bronchiolitis guidelines, defined as an acute respiratory illness with a combination of rhinitis, cough, tachypnoea, wheezing, crackles, or chest retractions. We excluded infants with a pre-existing heart and lung disease, immunodeficiency, immunosuppression, or gestational age of <32 weeks, those with a previous bronchiolitis hospitalization, or those who were transferred to a participating hospital >24 hours

after initial hospitalization. All patients were treated at the discretion of the treating physicians. The institutional review board at each participating hospital approved the study with a written informed consent obtained from the parent or guardian.

Of 921 infants enrolled into the longitudinal cohort, the current analysis investigated 244 infants hospitalized for bronchiolitis who were randomly selected for nasopharyngeal metatranscriptome (microbiome) and transcriptome (host) testing (**Figure 1** and **Supplementary Figure S1**).

Data Collection and Measurement of Virus, Metatranscriptome, and Transcriptome

Clinical data (patients' demographic characteristics, and family, environmental, and medical history, and details of the acute illness) were collected via structured interview and chart reviews using a standardized protocol. Additionally, nasopharyngeal airway specimens were collected within 24 hours of hospitalization using a standardized protocol [12]. The details of the data collection and measurement methods are described in the **Supplementary Methods**. The nasopharyngeal specimens were tested for a) respiratory viruses (e.g., respiratory syncytial virus [RSV] and rhinoviruses [RVs]), b) metatranscriptome (microbiome taxonomy at the species-level and function), and c) transcriptome (host function).

RNAseq for Nasopharyngeal Dual-transcriptome (Metatranscriptome and Transcriptome)

The details of RNA extraction, RNAseq, and quality control are described in the **Supplementary Methods**. Briefly, after total RNA extraction, DNase treatment, and rRNA reduction, we performed RNAseq with Illumina NovaSeq6000 using an S4 100PE Flowcell (Illumina, San Diego, CA). All RNAseq samples had high sequence coverage (a mean of 8,067,019 pair-end reads/sample) after quality control. We filtered and trimmed raw reads for adapters and contaminants using the *k*-mers strategy in bbduck. We characterized the active (via RNA transcripts) bacterial component of the microbiome (species-level) coupling PathoScope 2.0 with the expanded Human Oral Microbiome Database. To characterize the microbiome function, we used SUPER-FOCUS and Diamond. To annotate proteins that implement a specific biological process or structural complex into subsystems, we used the SEED database. This database comprises three-level hierarchical microbiome functions: the level 1 subsystem with 35 functions, followed by the level 2 subsystem with 194 functions and the level 3 subsystem with 1,290 functions. Lastly, we estimated host transcript abundances in Salmon using the human genome (hg38) and the mapping-based mode.

Functional and Clinical Outcomes

The outcomes of interest are a) host function (the nasopharyngeal transcriptome) at index hospitalization for bronchiolitis and b) asthma development by age 5 years. The definition of asthma was based on a commonly-used epidemiologic definition of asthma—physician-diagnosis of asthma by age 5 years, plus either asthma medication use (e.g., albuterol inhaler, inhaled corticosteroids, montelukast) or asthma-related symptoms in the preceding year.

Statistical Analysis

The objectives of the current study are a) to identify biologically distinct metatranscriptome profiles among infants with bronchiolitis (description [clustering]), and b) to relate them to the host transcriptome and the risk of asthma development (association). The analytic workflow is summarized in **Figure 1**. The details of the statistical analysis can be found in the **Supplementary Methods**.

Briefly, we first computed a distance matrix for each of three datasets—virus (including the genomic load of RSV, RV-A, and RV-C), microbiome taxonomy (species-level), and microbiome function data: Euclidean distance for the virus data, Bray-Curtis distance for the taxonomy data, and Pearson distance for the function data. Then, we computed an affinity matrix

of each dataset separately, and generated a fused affinity matrix by similarity network fusion using the *SNFtool* package. To identify mutually exclusive metatranscriptome profiles, we applied spectral clustering to the fused affinity matrix. To choose an optimal number of profiles, we used a combination of the silhouette scores **(Supplementary Figure S2, Panel A**), network modularity **(Supplementary Figure S2, Panel B**), profile size (n=33-67), and clinical and biological plausibility. The network modularity measures how well-separated subnetworks are given a particular partitioning (i.e., profiles) of the network. To test the stability of profiles (i.e., internal validation), we computed the accuracy of profiles using semi-supervised label propagation methods **(Supplementary Figure S3**). To complement these approaches, we also used *a priori* knowledge by confirming that the derived profiles are consistent with earlier studies [2].

After deriving the metatranscriptome profiles, we examined their relationships with both functional (host transcriptome) and clinical (asthma) outcomes. First, we conducted differential expression gene and functional pathway analyses by comparing the reference profile with each of the other profiles. To investigate whether genes for specific biological pathways are enriched among the large positive or negative fold changes, we conducted a functional class scoring analysis using *clusterProfiler* package. Second, to determine the longitudinal association of the profiles with asthma at age 5 years (binary outcome), we constructed unadjusted and adjusted

logistic regression models accounting for patient clustering within sites. In the sensitivity analysis, we examined the robustness of profile-outcome associations by repeating the analysis using a different number of profiles. We analysed the data using R version 3.6.1 (R Foundation for Statistical Computing, Vienna, Austria). All P-values were two-tailed, with $P<0.05$ considered statistically significant. We corrected for multiple testing using the Benjamini-Hochberg false discovery rate (FDR) method.

RESULTS

Of the infants enrolled into this longitudinal cohort, the current study focused on 244 randomly selected infants with bronchiolitis who underwent testing for nasopharyngeal airway microbial metatranscriptome and host transcriptome (**Figures 1** and **Supplementary Figure S1**). The analytic cohort and non-analytic cohorts did not differ in patient characteristics ($P \geq 0.05$; **Supplementary Table S2**), except for daycare use and solo-RSV infection. Among the analytic cohort, the median age was 3 (IQR, 2-6) months, 40.2% were female, and 41.8% were non-Hispanic white. Overall, 91.0% were RSV infection with solo-RSV infection in 65.2% and RSV/RV coinfection in 11.9% (**Table 1**).

Integrated Omics Approach Identified Distinct Metatranscriptome Profiles

To derive biologically distinct metatranscriptome profiles of infant bronchiolitis, we applied integrative network and clustering approaches to the virus, microbiome taxonomy (species-level), and microbiome function data (**Figure 1**). Both of the average silhouette scores and network modularity found that a 5-class model was the optimal fit (**Supplementary Figure S2**), with the 5 profiles called A, B, C, D, and E. The semi-supervised label propagation methods also indicated that the stability was also highest with the 5-class model (**Supplementary Figure S3**).

The 5 distinct metatranscriptome profiles (**Figure 2A** and **Supplementary Figure S4**) were chiefly characterized by the identified virus(es) and the major bacteria species of the nasopharyngeal airway microbiome: A) virus^{RSV}microbiome^{commensals} (27.5%), B) virus$^{RSV/RV\text{-}A}$microbiome$^{H.influenzae}$ (14.8%), C) virus^{RSV}microbiome$^{S.pneumoniae}$ (24.2%), D) virus^{RSV}microbiome$^{M.nonliquefaciens}$ (13.5%), and E) virus$^{RSV/RV\text{-}C}$microbiome$^{M.catarrhalis}$ (20.1%) (**Table 1**; **Figures 2B** and **3**).

Descriptively, infants with a profile A were characterized by a young age, a low proportion of parental asthma and eczema and personal history of eczema, and a high proportion of RSV infection (**Figures 2**, and **Supplementary Figures S5**, **S6**, and **S7**). In many respects they resembled "classic" bronchiolitis. These infants also had a higher abundance of commensals (e.g., *Corynebacterium*, *Cutibacterium*; both FDR<0.001; **Figure 3** and **Supplementary Figure S7**). Infants with a profile B were characterized by a high proportion of lifetime antibiotics use, history of eczema, parental eczema, IgE sensitization, and coinfection with RV-A, and a higher abundance of *H. influenzae* (FDR<0.001when compared to those with a profile A). Infants with a profile C were characterized by a high proportion of parental asthma and solo-RSV infection as well as a higher abundance of *S. pneumoniae* (FDR<0.001). Infants with a profile D were characterized by a low proportion of hypoxemia, a high proportion of RSV infection, and a higher abundance of *M. nonliquefaciens* (FDR<0.001). Infants with a profile E were

characterized by a high proportion of RV-C coinfection and a higher abundance of *M. catarrhalis* (FDR<0.001). These virus and microbiome variables that characterized the profiles had high-ranked normalized mutual information scores, indicating large contributions to the similarity network (**Supplementary Figure S8**).

Metatranscriptome Profiles Had Distinct Microbiome Function Pathways

These metatranscriptome profiles of infant bronchiolitis also had distinct microbiome functions. For example, compared to infants with profile A (virus^{RSV}microbiome^{commensals}) who clinically resembled "classic" bronchiolitis and were the largest group, those with a profile B (virus$^{RSV/RV-A}$microbiome$^{H.influenzae}$) had enriched virulence and iron acquisition and metabolism (FDR<0.05; **Figure 4**). More specifically, the profile B infants had an upregulated virulence function related to antibiotic resistance (e.g., multidrug resistance efflux pumps) (FDR<0.05; **Supplementary Figure S9A**) and iron metabolism function related to hemin transport (FDR<0.05; **Supplementary Figure S9B**). The profile C (virus^{RSV}microbiome$^{S.pneumoniae}$) infants had enriched fatty acid, lipid, and isoprenoid metabolism (FDR<0.05; **Figure 4**)—e.g., upregulated glycerolipid and glycerophospholipid metabolism (FDR<0.05; **Supplementary Figure S10**). In contrast, the profile D (virus^{RSV}microbiome$^{M.nonliquefaciens}$) infants had downregulated glycerolipid and glycerophospholipid function in fatty acid, lipid, and isoprenoid

metabolism (FDR<0.05; **Figure 4** and **Supplementary Figure S11**). Lastly, the profile E (virus$^{RSV/RV\text{-}C}$microbiome$^{M.catarrhalis}$) infants had upregulated stress response metabolism (FDR<0.05; **Figure 4**)—e.g., cold shock CspA protein family (FDR<0.05; **Supplementary Figure S12**).

Metatranscriptome Profiles Had Distinct Host Transcriptome Characteristics During Infancy and Differential Risk for Developing Asthma

To better understand the relationship between the metatranscriptome profiles and the host response (represented by the transcriptome) during infancy, we conducted differential expression gene and functional pathway analyses. Compared with the profile A, the profile B had 63 differentially enriched pathways (FDR<0.05; **Supplementary Figure S13**)—e.g., upregulated T_H17 and downregulated type I interferon pathways. Similarly, the profile C had 45 differentially enriched pathways (FDR<0.05)—e.g., an upregulated receptor for advanced glycation end products (RAGE) signalling pathway (**Supplementary Figure S14**). For the profiles A vs. D and A vs. E comparisons, the detailed differences are summarized in **Supplementary Figures S15** and **S16**.

The metatranscriptome profiles also had differential risks for developing asthma by age 5 years (**Figure 5**). For example, compared with profile A infants, profile B infants had a

significantly higher risk (17.9% vs. 38.9%; adjOR, 2.81; 95%CI, 1.11–7.26; P=0.030). Likewise, profile C infants also had a significantly higher risk of asthma (35.6%; adjOR, 2.49; 95%CI, 1.10–5.87; P=0.031) while profile D infants had a non-significantly lower risk of asthma (9.1%; adjOR, 0.47; 95%CI, 0.10–1.65; P=0.28). In the stratification by the development of recurrent wheeze by age 3 years, the results were similar (**Supplementary Figures S17**).

Sensitivity Analysis

To address the robustness of these findings, we examined different numbers of profiles. Alluvial plot (**Supplementary Figure S18**) demonstrates the consistency of the original profiles (profiles A-E) across the different numbers chosen (4 and 6 profiles). For example, with the use of 4-class models (that had the second-highest accuracy in label propagation methods), the first and fourth profiles had >90% concordance with the original profiles A and E (**Supplementary Table S3**). In contrast, the second profile had a mixture of the original profiles B and C. Similar to the primary analysis, these four profiles were also characterized by virus and microbiome taxonomy (e.g., *S. pneumoniae, M. catarrhalis*) (**Supplementary Table S3**; **Supplementary Figure S19**). Lastly, compared to profile 1 (which is concordant with profile A), profile 2 (concordant with profiles B and C) infants with distinct microbiome functions (e.g., enriched by

virulence, iron acquisition and metabolism, and fatty acid, lipid and isoprenoid metabolism; **Supplementary Figure S20**) had upregulated T_H17 (FDR=0.002) and RAGE signalling (FDR=0.001) pathways. These infants also had a significantly higher risk for developing asthma (18.8% vs. 34.6%; adjOR, 2.25; 95%CI, 1.05-5.00; P=0.041; **Supplementary Figure S21**).

DISCUSSION

By integrating the virus and nasopharyngeal metatranscriptome (both microbiome taxonomy and function) data from a multicentre prospective cohort study of 244 infants with severe bronchiolitis, we identified five biologically distinct metatranscriptome profiles. In particular, infants with profile B ($virus^{RSV/RV\text{-}A}microbiome^{H.influenzae}$) not only had distinct microbiome function (e.g., an upregulated virulence function) but also were associated with unique host response in the nasopharyngeal airway (e.g., upregulated T_H17 pathways) at the time of bronchiolitis. Additionally, infants with profile C ($virus^{RSV}microbiome^{S.pneumoniae}$) also had distinctive microbiome function (e.g., an enriched lipid metabolism) and host response (e.g., an upregulated RAGE signalling pathways). Furthermore, these two metatranscriptome profiles had a significantly higher risk for developing childhood asthma. To the best of our knowledge, this is the first study that has identified metatranscriptome profiles in bronchiolitis and demonstrated their relationship with host airway response and subsequent development of asthma.

Recent research has suggested the relationship between the virus, airway microbiome, host response, and respiratory disease. For example, studies have reported the association between respiratory viruses and unique upper airway microbiome (measured either via 16S rRNA gene sequencing or quantitative PCR) in infants with bronchiolitis [5, 6, 15] and school-age children [16]. In these studies, RV-A infection was associated with *Haemophilus*-dominant profile and RV-C with *Moraxella*-dominant profile, which is consistent with our metatranscriptomics findings. Recent studies have also shown the potential role of *Haemophilus* and *Streptococcus* genera in the upper airway—both among infants with or without bronchiolitis—in the host immune response [17, 18] and the development of wheeze illness and asthma [18–20]. Furthermore, research has suggested that the interaction of microbiome-host functions—via downstream metabolic regulation—contributes to the pathobiology of bronchiolitis and asthma [21]. Indeed, studies of upper airway metabolome among infants with bronchiolitis have reported the associations of altered lipid metabolism with disease severity [12] and asthma risk [21]. The current study corroborates these earlier reports, and extends them not only by identifying metatranscriptome profiles through the integrated omics approach but also by demonstrating their relationship with unique host immune response and asthma development.

There are several potential mechanisms linking the metatranscriptome profiles to the host airway response and subsequent asthma risk. First, we observed the relationship of profile B (virus$^{\text{RSV/RV-A}}$microbiome$^{\textit{H.influenzae}}$)—characterized by a high likelihood of previous antibiotics exposure, atopy/allergic sensitization, *H. influenzae* abundance, and enriched virulence related with antibiotic resistance and iron metabolism function—with upregulated T_H17 and downregulated type I interferon pathways. Consistently, study has reported that antibiotic exposures during early infancy lead to *Haemophilus*-dominant maturation of nasal microbiome during the first two years of life [22] . Likewise, RV-A infection is also associated with a high abundance of *Haemophilus* in young children [7, 16]. Additionally, *H. influenzae* requires hemin transport function and X factor for its aerobic growth [23]. Furthermore, animal models have reported that *H. influenzae* induces early IL-17 responses from lung macrophages and neutrophils, followed by later responses from Th17 cells in lungs and mediastinal lymph nodes, leading to neutrophil influx into the airways [24]. Studies have also shown the roles of T_H17 pathway in neutrophilic inflammation, steroid insensitivity, and airway remodelling in both allergic and non-allergic asthma [25, 26]. In addition to the upregulated T_H17 pathway, the profile B also had downregulated type I interferon pathways. Recent research has reported immature type I interferon response to RV-A infection [27]. Reduced anti-viral response (e.g., interferons) to RV infection impairs phagocytosis of *Haemophilus influenzae* among patients

with chronic lung disease [28]. Studies have also demonstrated that type I interferon response to RV infection is impaired among infants with allergic sensitization [29] and that the use of anti-IgE monoclonal antibody improves interferon-α response and reduces asthma exacerbation risks [30]. These prior data are in line with our findings in the profile B.

Second, the mechanisms linking profile C ($virus^{RSV}microbiome^{S.pneumoniae}$)—characterized by a high likelihood of solo-RSV infection, *S. pneumoniae* dominance, and enriched glycerolipid and glycerophospholipid metabolism—to the unique host response (e.g., RAGE signalling) and asthma risk warrants further clarification. Research has shown that RSV infection increases the virulence of *S. pneumoniae* [31]. *S. pneumoniae* produces phosphatidic acid, a precursor to all membrane glycerophospholipids [32]. Studies have also suggested the pro-inflammatory role of glycerophospholipid (e.g., activation of natural killer T cells) in the pathobiology of asthma [33, 34]. Additionally, *S. pneumoniae* is associated with an upregulated RAGE expression in the lung [35]. Mendelian randomization study has also demonstrated the causal role of RAGE in asthma pathobiology [36]. Furthermore, compared with RAGE knockout mice, wild mice have developed more pronounced airway inflammation and mucus metaplasia when intranasally administered recombinant type 2 cytokines [37]. While it is intriguing to observe the abundance of *S pneumoniae* and its potential pathobiological effect in the post-pneumococcal conjugate

vaccine (PCV) era, research has shown that the introduction of PCV-13 has led to the changes in pneumococcal serotypes, genotypes, and antimicrobial resistance [38].

In contrast, we observed that the profile D (virus^{RSV}microbiome$^{M.nonliquefaciens}$) was characterized by downregulated glycerolipid and glycerophospholipid function and had the lowest risk for developing asthma. Studies have reported that *M. nonliquefaciens* is less-pathogenic [39] and associated with a lower risk of incident asthma [40]. Besides, the low bronchiolitis severity (suggested by the low proportion of hypoxemia) in the profile D may also have contributed to the decreased asthma risk. Lastly, the profile E (virus$^{RSV/RV-C}$microbiome$^{M.catarrhalis}$) had upregulated Casp A family proteins, which induces *uspA1* gene expression and prolongs survival of *M. catarrhalis* [41]. *M. catarrhalis*'s lipopolysaccharides activate both MyD88-dependent and TRIF-dependent signaling pathways [42]. These pathways activate proinflammatory downstream signalling (e.g., NFκB, mitogen-activated protein kinases, interferon regulatory factors) that play roles in asthma [43]. Notwithstanding the complexity of these mechanisms, the observed interrelations between the metatranscriptome profiles, host immune response, and asthma development are important findings. Our data should not only advance research that will disentangle the complex web but they also inform the development of microbiome- (or endotype-) specific strategies for the primary prevention of asthma.

Our study has several potential limitations. First, bronchiolitis involves inflammation of the lower airways in addition to the upper airways. While the present study is based on nasopharyngeal samples, studies have shown that upper airway sampling provides a reliable representation of the lung microbiome [43] and transcriptome [44]. Furthermore, the use of upper airway specimens is preferable because lower airway sampling (e.g., bronchoscopy) would be quite invasive in young infants. Second, the nasopharyngeal samples were obtained at a single time-point. While longitudinal molecular data are also informative, the study objective was to identify metatranscriptome profiles of bronchiolitis. However, even with single-time point data, we successfully identified biologically distinct profiles that are longitudinally associated with asthma risk. Third, it is possible that asthma diagnosis is misclassified and that some children are going to develop asthma at a later age. To address these points, the study sample is currently being followed up to age 9 years. Fourth, the present study did not have healthy "controls". However, our study objective was not to evaluate metatranscriptome profiles related to bronchiolitis development (i.e., bronchiolitis yes vs. no) but to examine the relationship between the metatranscriptome profile of infants with bronchiolitis and their asthma risk. Fifth, while this hypothesis-generating study derives novel and well-calibrated hypotheses that facilitate future experiments, our findings warrant further validation. Lastly, the study sample consisted of racially/ethnically and geographically diverse infants hospitalized for bronchiolitis. Our findings

may not be generalizable to infants with mild-to-moderate bronchiolitis or a sample with different respiratory virus proportions. Regardless, our data remain relevant for the 110,000 infants hospitalized yearly in the U.S. [1], a vulnerable population with substantial morbidity burden.

CONCLUSION

In summary, by applying an integrated omics approach to data from a multicentre prospective cohort of 244 infants with severe bronchiolitis, we identified five biologically distinct and clinically meaningful metatranscriptome profiles. These profiles were associated not only with distinct host airway response during bronchiolitis but also with differential risks for developing asthma. Our data suggest a complex interplay between the respiratory virus, airway microbiome, and host immune response, and their integrated contributions to the subsequent development of asthma. For clinicians, our findings may provide an evidence base for the early identification of high-risk children during an important period of airway development—early infancy. For researchers, our data should facilitate further investigations into the development of microbiome profile (or endotype)-specific strategies for asthma prevention.

Acknowledgments: This study was supported by grants from the National Institutes of Health (Bethesda, MD): U01 AI-087881, R01 AI-114552, R01 AI-108588, R01 AI-134940, and UG3/UH3 OD-023253. M.P.-L. was partially supported by the Margaret Q. Landenberger Research Foundation, the NIH National Center for Advancing Translational Sciences (Award Number UL1TR001876), and the Fundação para a Ciência e a Tegnologia (T495756868-00032862). The content of this manuscript is solely the responsibility of the authors and does not necessarily represent the official views of the National Institutes of Health. The funding organizations were not involved in the collection, management, or analysis of the data; preparation or approval of the manuscript; or decision to submit the manuscript for publication.

We thank the MARC-35 study hospitals and research personnel for their ongoing dedication to bronchiolitis and asthma research (**Supplementary Table S1** in the **Supplementary Materials**), and Ashley F. Sullivan, MS, MPH and Janice A. Espinola, MPH (Massachusetts General Hospital, Boston, MA) for their many contributions to the MARC-35 study. We also thank Alkis Togias, MD, at the National Institutes of Health (Bethesda, MD) for helpful comments about the study results.

REFERENCES

1. Fujiogi M, Goto T, Yasunaga H, Fujishiro J, Mansbach JM, Camargo CA, Hasegawa K. Trends in bronchiolitis hospitalizations in the United States: 2000-2016. *Pediatrics* 2019; 144.

2. Hasegawa K, Dumas O, Hartert TV, Camargo CA. Advancing our understanding of infant bronchiolitis through phenotyping and endotyping: clinical and molecular approaches. *Expert Rev Respir Med* 2016; 10: 891–899.

3. Ralston SL, Lieberthal AS, Meissner HC, Alverson BK, Baley JE, Gadomski AM, Johnson DW, Light MJ, Maraqa NF, Mendonca EA, Phelan KJ, Zorc JJ, Stanko-Lopp D, Brown MA, Nathanson I, Rosenblum E, Sayles S, Hernandez-Cancio S, American Academy of Pediatrics. Clinical practice guideline: the diagnosis, management, and prevention of bronchiolitis. *Pediatrics* 2014; 134: e1474-1502.

4. Dumas O, Hasegawa K, Mansbach JM, Sullivan AF, Piedra PA, Camargo CA. Severe bronchiolitis profiles and risk of recurrent wheeze by age 3 years. *J. Allergy Clin. Immunol.* 2019; 143: 1371-1379.e7.

5. Rosas-Salazar C, Shilts MH, Tovchigrechko A, Schobel S, Chappell JD, Larkin EK, Shankar J, Yooseph S, Nelson KE, Halpin RA, Moore ML, Anderson LJ, Peebles RS, Das SR, Hartert TV. Differences in the nasopharyngeal microbiome during acute respiratory tract infection with human rhinovirus and respiratory syncytial virus in infancy. *J. Infect. Dis.* 2016; 214: 1924–1928.

6. Mansbach JM, Hasegawa K, Henke DM, Ajami NJ, Petrosino JF, Shaw CA, Piedra PA, Sullivan AF, Espinola JA, Camargo CA. Respiratory syncytial virus and rhinovirus severe bronchiolitis are associated with distinct nasopharyngeal microbiota. *J Allergy Clin Immunol* 2016; 137: 1909-1913.e4.

7. Toivonen L, Camargo CA, Gern JE, Bochkov YA, Mansbach JM, Piedra PA, Hasegawa K. Association between rhinovirus species and nasopharyngeal microbiota in infants with severe bronchiolitis. *J. Allergy Clin. Immunol.* 2019; 143: 1925-1928.e7.

8. Rosas-Salazar C, Shilts MH, Tovchigrechko A, Schobel S, Chappell JD, Larkin EK, Gebretsadik T, Halpin RA, Nelson KE, Moore ML, Anderson LJ, Peebles RS, Das SR, Hartert TV. Nasopharyngeal Lactobacillus is associated with a reduced risk of childhood wheezing illnesses following acute respiratory syncytial virus infection in infancy. *J Allergy Clin Immunol* 2018; 142: 1447-1456.e9.

9. Turi KN, Shankar J, Anderson LJ, Rajan D, Gaston K, Gebretsadik T, Das SR, Stone C, Larkin EK, Rosas-Salazar C, Brunwasser SM, Moore ML, Peebles RS, Hartert TV. Infant viral respiratory infection nasal immune-response patterns and their association with subsequent childhood recurrent wheeze. *Am. J. Respir. Crit. Care Med.* 2018; 198: 1064–1073.

10. Raita Y, Camargo CA, Bochkov YA, Celedón JC, Gern JE, Mansbach JM, Rhee EP, Freishtat RJ, Hasegawa K. Integrated-omics endotyping of infants with rhinovirus bronchiolitis and risk of childhood asthma. *J Allergy Clin Immunol* 2021; 147: 2108–2117.

11. Hasegawa K, Mansbach JM, Ajami NJ, Petrosino JF, Freishtat RJ, Teach SJ, Piedra PA, Camargo CA. The relationship between nasopharyngeal CCL5 and microbiota on disease severity among infants with bronchiolitis. *Allergy* 2017; 72: 1796–1800.

12. Stewart CJ, Mansbach JM, Wong MC, Ajami NJ, Petrosino JF, Camargo CA, Hasegawa K. Associations of nasopharyngeal metabolome and microbiome with severity among infants with bronchiolitis. A Multiomic Analysis. *Am. J. Respir. Crit. Care Med.* 2017; 196: 882–891.

13. Fujiogi M, Camargo CA, Raita Y, Bochkov YA, Gern JE, Mansbach JM, Piedra PA, Hasegawa K. Association of rhinovirus species with nasopharyngeal metabolome in bronchiolitis infants: A multicenter study. *Allergy* 2020; 75: 2379–2383.

14. Tang HHF, Lang A, Teo SM, Judd LM, Gangnon R, Evans MD, Lee KE, Vrtis R, Holt PG, Lemanske RF, Jackson DJ, Holt KE, Inouye M, Gern JE. Developmental patterns in the nasopharyngeal microbiome during infancy are associated with asthma risk. *J Allergy Clin Immunol* 2021; 147: 1683–1691.

15. Stewart CJ, Mansbach JM, Piedra PA, Toivonen L, Camargo CA, Hasegawa K. Association of respiratory viruses with serum metabolome in infants with severe bronchiolitis. *Pediatr Allergy Immunol* 2019; 30: 848–851.

16. Bashir H, Grindle K, Vrtis R, Vang F, Kang T, Salazar L, Anderson E, Pappas T, Gangnon R, Evans MD, Jackson DJ, Lemanske RF, Bochkov YA, Gern JE. Association of rhinovirus species with common cold and asthma symptoms and bacterial pathogens. *J. Allergy Clin. Immunol.* 2018; 141: 822-824.e9.

17. Følsgaard NV, Schjørring S, Chawes BL, Rasmussen MA, Krogfelt KA, Brix S, Bisgaard H. Pathogenic bacteria colonizing the airways in asymptomatic neonates stimulates topical inflammatory mediator release. *Am. J. Respir. Crit. Care Med.* 2013; 187: 589–595.

18. Larsen JM, Brix S, Thysen AH, Birch S, Rasmussen MA, Bisgaard H. Children with asthma by school age display aberrant immune responses to pathogenic airway bacteria as infants. *J. Allergy Clin. Immunol.* 2014; 133: 1008–1013.

19. Mansbach JM, Luna PN, Shaw CA, Hasegawa K, Petrosino JF, Piedra PA, Sullivan AF, Espinola JA, Stewart CJ, Camargo CA. Increased Moraxella and Streptococcus species abundance after severe bronchiolitis is associated with recurrent wheezing. *J. Allergy Clin. Immunol.* 2020; 145: 518-527.e8.

20. Bisgaard H, Hermansen MN, Buchvald F, Loland L, Halkjaer LB, Bønnelykke K, Brasholt M, Heltberg A, Vissing NH, Thorsen SV, Stage M, Pipper CB. Childhood asthma after bacterial colonization of the airway in neonates. *N. Engl. J. Med.* 2007; 357: 1487–1495.

21. Fujiogi M, Camargo CA, Raita Y, Zhu Z, Celedón JC, Mansbach JM, Spergel JM, Hasegawa K. Integrated associations of nasopharyngeal and serum metabolome with bronchiolitis severity and asthma: A multicenter prospective cohort study. *Pediatr Allergy Immunol* 2021; 32: 905–916.

22. Raita Y, Toivonen L, Schuez-Havupalo L, Karppinen S, Waris M, Hoffman KL, Camargo CA, Peltola V, Hasegawa K. Maturation of nasal microbiota and antibiotic exposures during early childhood: a population-based cohort study. *Clin Microbiol Infect* 2021; 27: 283.e1-283.e7.

23. Whitby PW, Seale TW, VanWagoner TM, Morton DJ, Stull TL. The iron/heme regulated genes of Haemophilus influenzae: comparative transcriptional profiling as a tool to define the species core modulon. *BMC Genomics* 2009; 10: 6.

24. Essilfie A-T, Simpson JL, Horvat JC, Preston JA, Dunkley ML, Foster PS, Gibson PG, Hansbro PM. Haemophilus influenzae infection drives IL-17-mediated neutrophilic allergic airways disease. *PLoS Pathog* 2011; 7: e1002244.

25. Chesné J, Braza F, Mahay G, Brouard S, Aronica M, Magnan A. IL-17 in severe asthma. Where do we stand? *Am J Respir Crit Care Med* 2014; 190: 1094–1101.

26. Ricciardolo FLM, Sorbello V, Folino A, Gallo F, Massaglia GM, Favatà G, Conticello S, Vallese D, Gani F, Malerba M, Folkerts G, Rolla G, Profita M, Mauad T, Di Stefano A, Ciprandi G. Identification of IL-17F/frequent exacerbator endotype in asthma. *J Allergy Clin Immunol* 2017; 140: 395–406.

27. Wark PAB, Grissell T, Davies B, See H, Gibson PG. Diversity in the bronchial epithelial cell response to infection with different rhinovirus strains. *Respirology* 2009; 14: 180–186.

28. Finney LJ, Belchamber KBR, Fenwick PS, Kemp SV, Edwards MR, Mallia P, Donaldson G, Johnston SL, Donnelly LE, Wedzicha JA. Human rhinovirus impairs the innate immune response to bacteria in alveolar macrophages in chronic obstructive pulmonary disease. *Am J Respir Crit Care Med* 2019; 199: 1496–1507.

29. Durrani SR, Montville DJ, Pratt AS, Sahu S, DeVries MK, Rajamanickam V, Gangnon RE, Gill MA, Gern JE, Lemanske RF, Jackson DJ. Innate immune responses to rhinovirus are reduced by the high-affinity IgE receptor in allergic asthmatic children. *J Allergy Clin Immunol* 2012; 130: 489–495.

30. Teach SJ, Gill MA, Togias A, Sorkness CA, Arbes SJ, Calatroni A, Wildfire JJ, Gergen PJ, Cohen RT, Pongracic JA, Kercsmar CM, Khurana Hershey GK, Gruchalla RS, Liu AH, Zoratti EM, Kattan M, Grindle KA, Gern JE, Busse WW, Szefler SJ. Preseasonal treatment with either omalizumab or an inhaled corticosteroid boost to prevent fall asthma exacerbations. *J Allergy Clin Immunol* 2015; 136: 1476–1485.

31. Smith CM, Sandrini S, Datta S, Freestone P, Shafeeq S, Radhakrishnan P, Williams G, Glenn SM, Kuipers OP, Hirst RA, Easton AJ, Andrew PW, O'Callaghan C. Respiratory syncytial virus increases the virulence of Streptococcus pneumoniae by binding to penicillin binding protein 1a. A new paradigm in respiratory infection. *Am. J. Respir. Crit. Care Med.* 2014; 190: 196–207.

32. Gullett JM, Cuypers MG, Frank MW, White SW, Rock CO. A fatty acid-binding protein of Streptococcus pneumoniae facilitates the acquisition of host polyunsaturated fatty acids. *J Biol Chem* 2019; 294: 16416–16428.

33. Fazlollahi M, Lee TD, Andrade J, Oguntuyo K, Chun Y, Grishina G, Grishin A, Bunyavanich S. The nasal microbiome in asthma. *J Allergy Clin Immunol* 2018; 142: 834-843.e2.

34. Kinjo Y, Wu D, Kim G, Xing G-W, Poles MA, Ho DD, Tsuji M, Kawahara K, Wong C-H, Kronenberg M. Recognition of bacterial glycosphingolipids by natural killer T cells. *Nature* 2005; 434: 520–525.

35. van Zoelen MAD, Schouten M, de Vos AF, Florquin S, Meijers JCM, Nawroth PP, Bierhaus A, van der Poll T. The receptor for advanced glycation end products impairs host defense in pneumococcal pneumonia. *J Immunol* 2009; 182: 4349–4356.

36. Raita Y, Zhu Z, Freishtat RJ, Fujiogi M, Liang L, Patregnani JT, Camargo CA, Hasegawa K. Soluble receptor for advanced glycation end products (sRAGE) and asthma: Mendelian randomisation study. *Pediatr Allergy Immunol* 2021; 32: 1100–1103.

37. Perkins TN, Oczypok EA, Dutz RE, Donnell ML, Myerburg MM, Oury TD. The receptor for advanced glycation end products is a critical mediator of type 2 cytokine signaling in the lungs. *J Allergy Clin Immunol* 2019; 144: 796-808.e12.

38. Lo SW, Gladstone RA, van Tonder AJ, Lees JA, du Plessis M, Benisty R, Givon-Lavi N, Hawkins PA, Cornick JE, Kwambana-Adams B, Law PY, Ho PL, Antonio M, Everett DB, Dagan R, von Gottberg A, Klugman KP, McGee L, Breiman RF, Bentley SD, Global Pneumococcal Sequencing Consortium. Pneumococcal lineages associated with serotype replacement and antibiotic resistance in childhood invasive pneumococcal disease in the post-PCV13 era: an international whole-genome sequencing study. *Lancet Infect Dis* 2019; 19: 759–769.

39. LaCroce SJ, Wilson MN, Romanowski JE, Newman JD, Jhanji V, Shanks RMQ, Kowalski RP. Moraxella nonliquefaciens and M. osloensis are important Moraxella species that cause ocular infections. *Microorganisms* 2019; 7.

40. Raita Y, Pérez-Losada M, Freishtat RJ, Harmon B, Mansbach JM, Piedra PA, Zhu Z, Camargo CA, Hasegawa K. Integrated omics endotyping of infants with respiratory syncytial virus bronchiolitis and risk of childhood asthma. *Nat Commun* 2021; 12: 3601.

41. Heiniger N, Spaniol V, Troller R, Vischer M, Aebi C. A reservoir of Moraxella catarrhalis in human pharyngeal lymphoid tissue. *J Infect Dis* 2007; 196: 1080–1087.

42. Hassan F. Molecular mechanisms of moraxella catarrhalis-induced otitis media. *Curr Allergy Asthma Rep* 2013; 13: 512–517.

43. Marsh RL, Kaestli M, Chang AB, Binks MJ, Pope CE, Hoffman LR, Smith-Vaughan HC. The microbiota in bronchoalveolar lavage from young children with chronic lung disease includes taxa present in both the oropharynx and nasopharynx. *Microbiome* 2016; 4: 37.

44. Poole A, Urbanek C, Eng C, Schageman J, Jacobson S, O'Connor BP, Galanter JM, Gignoux CR, Roth LA, Kumar R, Lutz S, Liu AH, Fingerlin TE, Setterquist RA, Burchard EG, Rodriguez-Santana J, Seibold MA. Dissecting childhood asthma with nasal transcriptomics distinguishes subphenotypes of disease. *J. Allergy Clin. Immunol.* 2014; 133: 670-678.e12.

Table 1. Baseline characteristics and clinical course of infants with bronchiolitis, according to metatranscriptome profiles

Characteristics	Overall (n=244; 100%)	Profile A (n=67; 27.5%)	Profile B (n=36; 14.8%)	Profile C (n=59; 24.2%)	Profile D (n=33; 13.5%)	Profile E (n=49; 20.1%)	P-value
Demographics							
Age (month), median (IQR)	3 (2–6)	3 (1–6)	4 (2–7)	3 (2–6)	4 (2–7)	3 (2–6)	0.36
Female sex	98 (40.2)	29 (43.3)	13 (36.1)	22 (37.3)	17 (51.5)	17 (34.7)	0.54
Race/ethnicity							0.33
Non-Hispanic white	102 (41.8)	29 (43.3)	14 (38.9)	21 (35.6)	16 (48.5)	22 (44.9)	
Non-Hispanic black	57 (23.4)	12 (17.9)	6 (16.7)	21 (35.6)	8 (24.2)	10 (20.4)	
Hispanic	76 (31.1)	24 (35.8)	15 (41.7)	15 (25.4)	9 (27.3)	13 (26.5)	
Other or unknown	9 (3.7)	2 (3.0)	1 (2.8)	2 (3.4)	0 (0.0)	4 (8.2)	
Prematurity (32-36.9 weeks)	47 (19.3)	15 (22.4)	6 (16.7)	11 (18.6)	9 (27.3)	6 (12.2)	0.48
Birth weight (kg), median (IQR)	3.20 (2.89–3.57)	3.20 (2.90–3.52)	3.17 (2.70–3.42)	3.23 (2.86–3.69)	3.09 (2.79–3.43)	3.31 (3.00–3.64)	0.43
Mode of birth (caesarean delivery)	84 (35.0)	19 (28.8)	15 (42.9)	22 (37.3)	11 (33.3)	17 (36.2)	0.69
Previous breathing problems							0.92
0	204 (83.6)	55 (82.1)	31 (86.1)	50 (84.7)	27 (81.8)	41 (83.7)	
1	30 (12.3)	8 (11.9)	3 (8.3)	8 (13.6)	4 (12.1)	7 (14.3)	
2	10 (4.1)	4 (6.0)	2 (5.6)	1 (1.7)	2 (6.1)	1 (2.0)	
Previous ICU admission	4 (1.6)	3 (4.5)	0 (0.0)	0 (0.0)	1 (3.0)	0 (0.0)	0.19
History of eczema	31 (12.7)	3 (4.5)	8 (22.2)	10 (16.9)	2 (6.1)	8 (16.3)	0.03
Palivizumab use	8 (3.8)	1 (1.7)	2 (6.2)	3 (6.1)	0 (0.0)	2 (4.9)	0.48
Lifetime antibiotic use*	79 (32.4)	25 (37.3)	17 (47.2)	16 (27.1)	4 (12.1)	17 (34.7)	0.02
Ever attended daycare	71 (29.1)	15 (22.4)	11 (30.6)	16 (27.1)	13 (39.4)	16 (32.7)	0.46
Cigarette smoke exposure at home	34 (13.9)	9 (13.4)	4 (11.1)	11 (18.6)	6 (18.2)	4 (8.2)	0.52
Maternal smoking during pregnancy	34 (14.2)	9 (13.6)	7 (20.0)	7 (11.9)	3 (9.1)	8 (17.0)	0.69
Parental history of asthma	76 (31.1)	14 (20.9)	12 (33.3)	24 (40.7)	11 (33.3)	15 (30.6)	0.19
Parental history of eczema	46 (18.9)	9 (13.4)	12 (33.3)	12 (20.3)	8 (24.2)	5 (10.2)	0.06
Clinical presentation							
Weight (kg), median (IQR)	6.07 (4.60–7.99)	5.50 (4.36–7.10)	6.80 (5.16–8.12)	6.28 (4.52–7.53)	6.40 (4.75–8.20)	6.20 (4.80–8.45)	0.22
Respiratory rate (per minute), median (IQR)	48 (40–60)	48 (40–56)	48 (40–56)	48 (39– 60)	52 (44–64)	50 (41–60)	0.45
Oxygen saturation							0.19
<90%	29 (12.2)	12 (19.0)	4 (11.8)	4 (6.8)	2 (6.2)	7 (14.3)	
90-93%	190 (80.2)	46 (73.0)	26 (76.5)	53 (89.8)	29 (90.6)	36 (73.5)	
≥94%	18 (7.6)	5 (7.9)	4 (11.8)	2 (3.4)	1 (3.1)	6 (12.2)	
Blood eosinophilia (≥4%)	21 (10.1)	4 (7.0)	4 (13.3)	5 (10.0)	2 (6.9)	6 (14.3)	0.73

IgE sensitization	51 (20.9)	11 (16.4)	9 (25.0)	13 (22.0)	6 (18.2)	12 (24.5)	0.77
Clinical course							
Positive pressure ventilation use †	18 (7.4)	6 (9.0)	3 (8.3)	5 (8.5)	3 (9.1)	1 (2.0)	0.55
Intensive treatment use‡	42 (17.2)	13 (19.4)	6 (16.7)	12 (20.3)	3 (9.1)	8 (16.3)	0.72
Length-of-day (day), median (IQR)	2 (1-3)	2 (1–4)	2 (1–4)	2 (1–4)	2 (1–3)	2 (1–3)	0.89
Antibiotic use during hospitalization	80 (32.8)	26 (38.8)	15 (41.7)	19 (32.2)	8 (24.2)	12 (24.5)	0.29
Corticosteroid use during	29 (11.9)	8 (11.9)	7 (19.4)	10 (16.9)	1 (3.0)	3 (6.1)	0.11
Respiratory virus							
RSV infection	222 (91.0)	61 (91.0)	31 (86.1)	59 (100.0)	33 (100.0)	38 (77.6)	<0.001
RSV-A§	153 (62.7)	46 (68.7)	22 (61.1)	41 (69.5)	15 (45.5)	29 (59.2)	0.15
RSV-B§	71 (29.1)	16 (23.9)	9 (25.0)	19 (32.2)	18 (54.5)	9 (18.4)	0.01
Solo-RSV infection	159 (65.2)	42 (62.7)	21 (58.3)	48 (81.4)	24 (72.7)	24 (49.0)	0.007
RV infection							
RV-A	26 (10.7)	8 (11.9)	7 (19.4)	5 (8.5)	2 (6.1)	4 (8.2)	0.41
RV-B	4 (1.6)	1 (1.5)	1 (2.8)	0 (0.0)	1 (3.0)	1 (2.0)	0.67
RV-C	21 (8.6)	2 (3.0)	0 (0.0)	1 (1.7)	2 (6.1)	16 (32.7)	<0.001
Solo-RV infection	13 (5.3)	4 (6.0)	1 (2.8)	0 (0.0)	0 (0.0)	8 (16.3)	0.002
RSV/RV coinfection	29 (11.9)	5 (7.5)	3 (8.3)	6 (10.2)	5 (15.2)	10 (20.4)	0.25
Other coinfection pathogens with RSV¶	34 (13.9)	14 (20.9)	7 (19.4)	5 (8.5)	4 (12.1)	4 (8.2)	0.17
Chronic outcome							
Asthma at age 5 years	62 (25.4)	12 (17.9)	14 (38.9)	21 (35.6)	3 (9.1)	12 (24.5)	0.009

Abbreviations: IQR, interquartile range; ICU, intensive care unit; RSV, respiratory syncytial virus; RV, rhinovirus; IgE, immunoglobulin E

Data are no. (%) of infants unless otherwise indicated. Percentages may not equal 100, because of rounding and missingness.

* Any systemic antibiotic use from birth up to the index hospitalization for bronchiolitis.

† Infants with bronchiolitis who underwent continuous positive airway ventilation and/or mechanical ventilation.

‡ Infants with bronchiolitis who were admitted to ICU and/or who underwent positive pressure ventilation.

§ Two infants had coinfection of RSV-A and -B.

¶ Infants with coinfection of RSV and non-RV virus(es) include adenovirus infection (n=7), bocavirus (n=8), endemic coronavirus (n=15), enterovirus (n=1), influenza virus (n=1), human metapneumovirus (n=4), *Mycoplasma pneumonia* (n=1), and parainfluenza virus (n=3). Since 6 infants have co-infection with ≥3 infecting agents, the total number is not equal to 34.

FIGURE LEGENDS

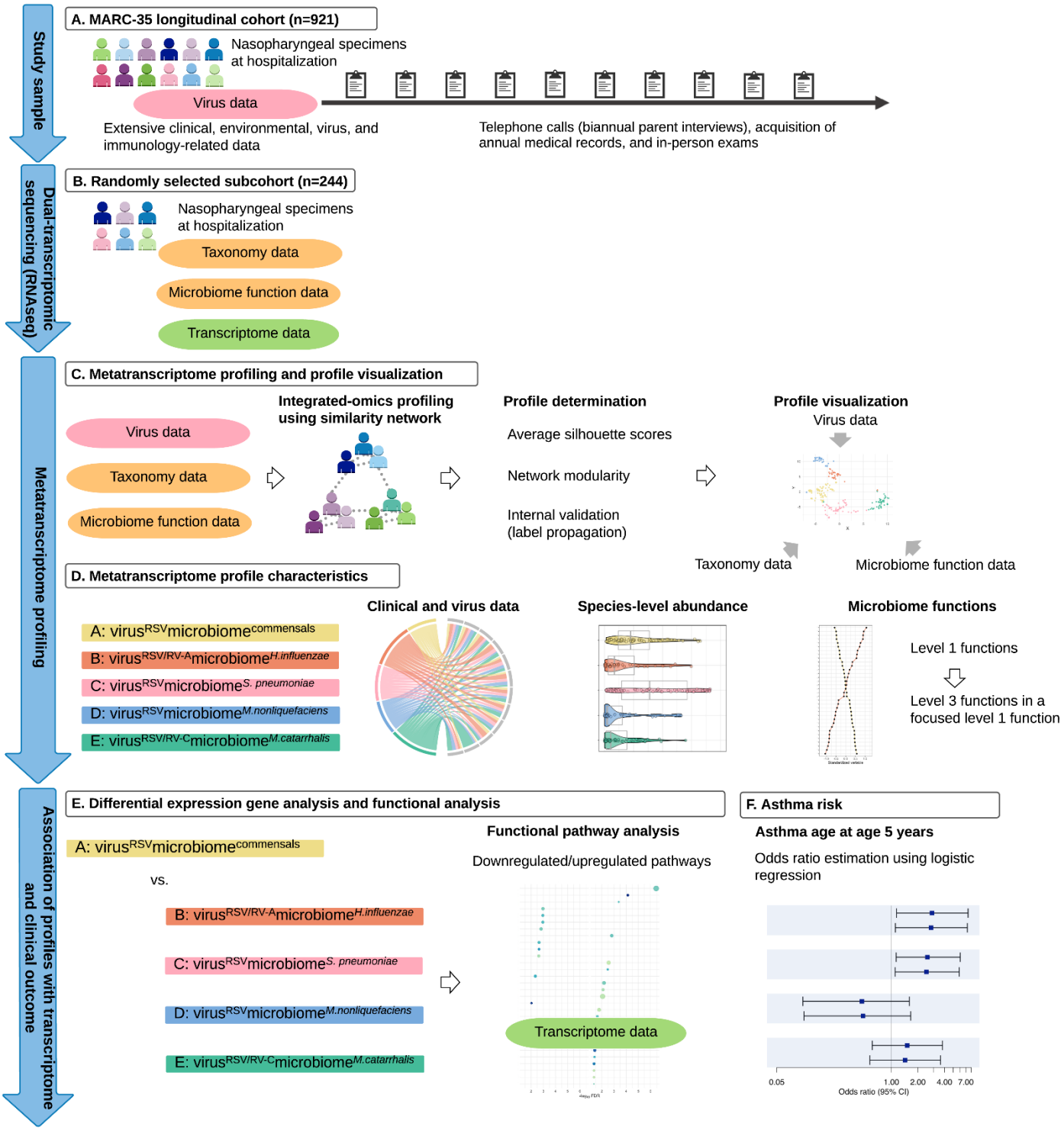

Figure 1. Analytic workflow of metatranscriptome profiling

A. A total of 921 infants (age <1 year) hospitalized with bronchiolitis comprised the MARC-35 longitudinal cohort. At enrolment, the nasopharyngeal specimens were collected. These nasopharyngeal specimens were

tested for respiratory viruses (e.g., RSV, RV species) and dual-transcriptome sequencing. These infants are followed with biannual parent interviews, acquisition of annual medical records, and in-person exams.

B. Randomly-selected 244 infants underwent dual-transcriptome sequencing (via RNAseq) of nasopharyngeal specimens to characterize the microbiome taxonomy and function as well as the host transcriptome.

C. After individually computing an affinity matrix for each of three datasets (i.e., virus, microbiome taxonomy and function data), we generated a fused affinity matrix by similarity network fusion. Then, we used the fused affinity matrix to identify metatranscriptome profiles by spectral clustering. To choose an optimal number of profiles, we used a combination of silhouette scores, network modularity, profile size, and clinical and biological plausibility. We visualized the five profiles by using the t-distributed stochastic neighbour embedding (t-sne) method.

D. To visualize the between-metatranscriptome profile differences in the major clinical and virus variables, microbiome taxonomy, and functions, we used chord diagrams, pirate plots, and ranked plots.

E. To examine the relationship between the metatranscriptome profiles and host function (transcriptome data), we performed differential gene expression analyses and functional pathway analyses. As infants with a profile A clinically resembled “classic” bronchiolitis and had the largest profile size, this group served as the reference group.

F. To examine the relationship of the metatranscriptome profiles with the risk for developing asthma (binary outcome), we constructed unadjusted and adjusted logistic regression models.

Abbreviations: RSV, respiratory syncytial virus; RV-A, rhinovirus A; RV-C, rhinovirus C

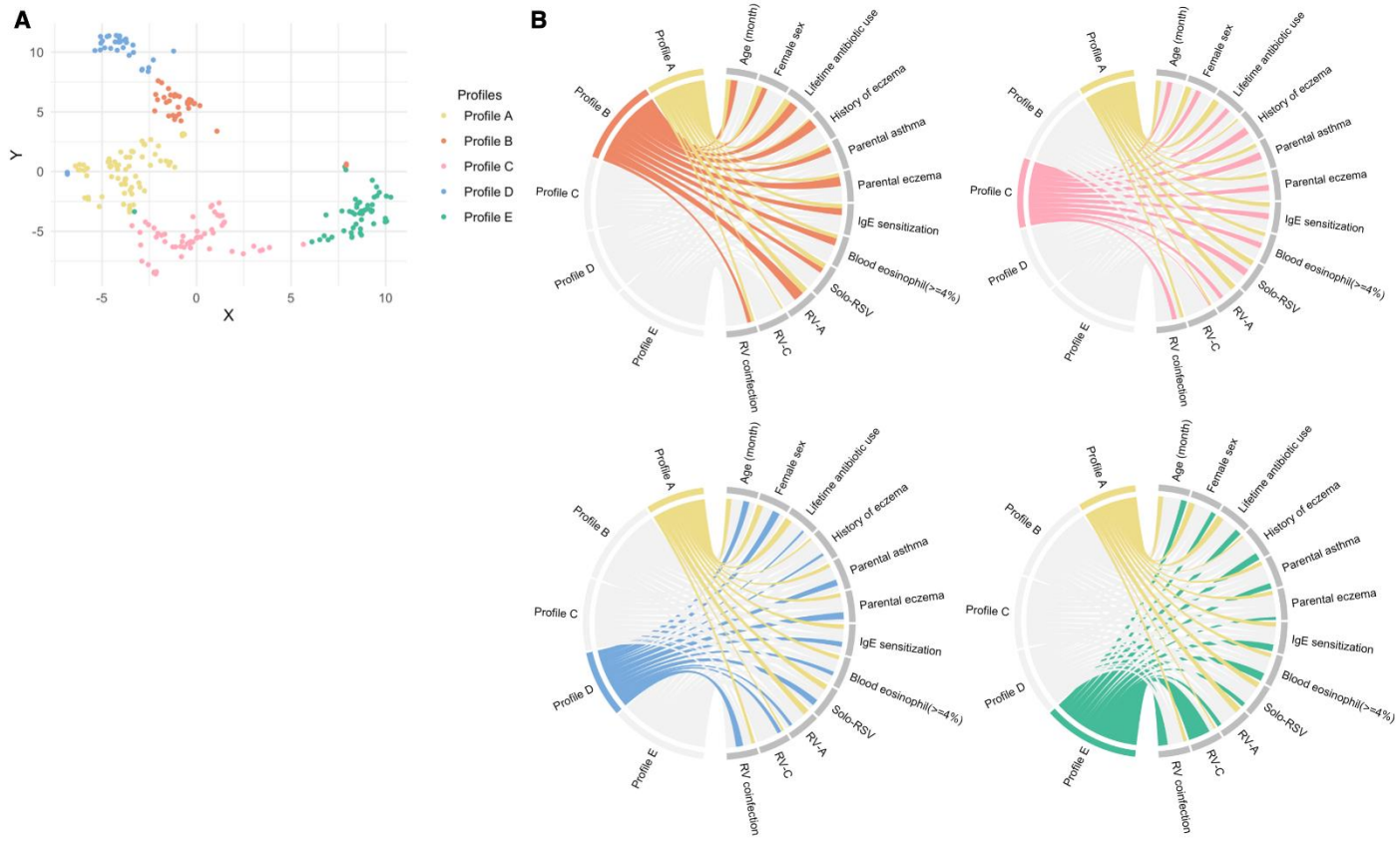

Figure 2. Metatranscriptome profiles among infants with bronchiolitis, and their relationship with major clinical and virus variables

A. T-distributed stochastic neighbor embedding of nasopharyngeal metatranscriptome profiles

To visualize the metatranscriptome profiles, the t-distributed stochastic neighbour embedding method was applied to the five eigenvectors in the spectral clustering. Each dot represents the metatranscriptome of a single infant in a low-dimensional space. The infants cluster together according to their metatranscriptome profiles.

B. Major clinical and virus characteristics according to metatranscriptome profiles

The ribbons connect from the individual metatranscriptome profiles to the major clinical and virus characteristics. The width of the ribbon represents the proportion of infants within the profile who have the corresponding clinical or virus characteristic, which was scaled to a total of 100%. For example, the profile B infants (light orange) had a high proportion of lifetime antibiotics use, history of eczema, parental eczema, IgE

sensitization, blood eosinophilia, and coinfection with RV-A. Profile C (pink) infants had a high proportion of parental asthma and solo-RSV infection.

Abbreviations: IgE, immunoglobulin E; RSV, respiratory syncytial virus; RV, rhinovirus; RV-A, rhinovirus A; RV-C, rhinovirus C

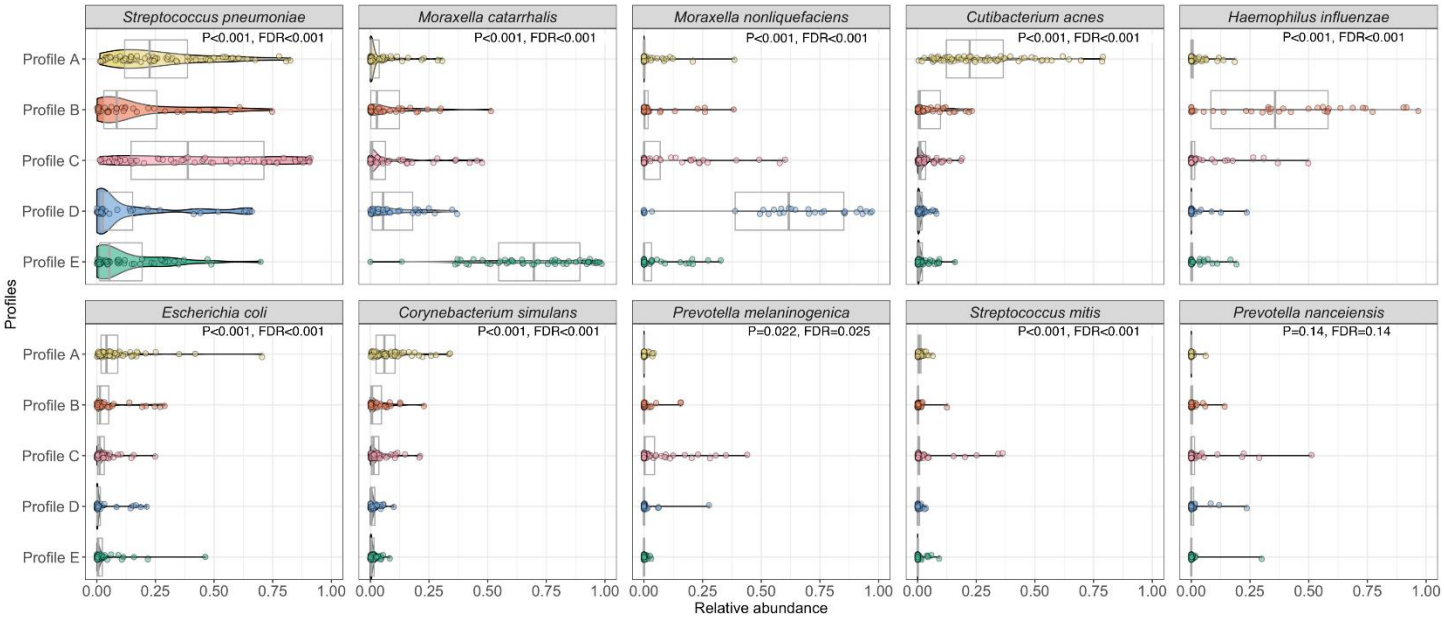

Figure 3. Between-profile differences in relative abundance of ten most abundant nasopharyngeal microbial species among infants with bronchiolitis

The pirate plots (a combination of boxplots and violin plots) show the distribution of the ten most abundant species in the nasopharyngeal microbiome, according to the five metatranscriptome profiles. In the overlying violin plots, the width represents the probability that infants in a profile take on a specific relative abundance. The between-profile differences in the relative abundance were tested by Kruskal-Wallis test.

Abbreviation: FDR, false discovery rate

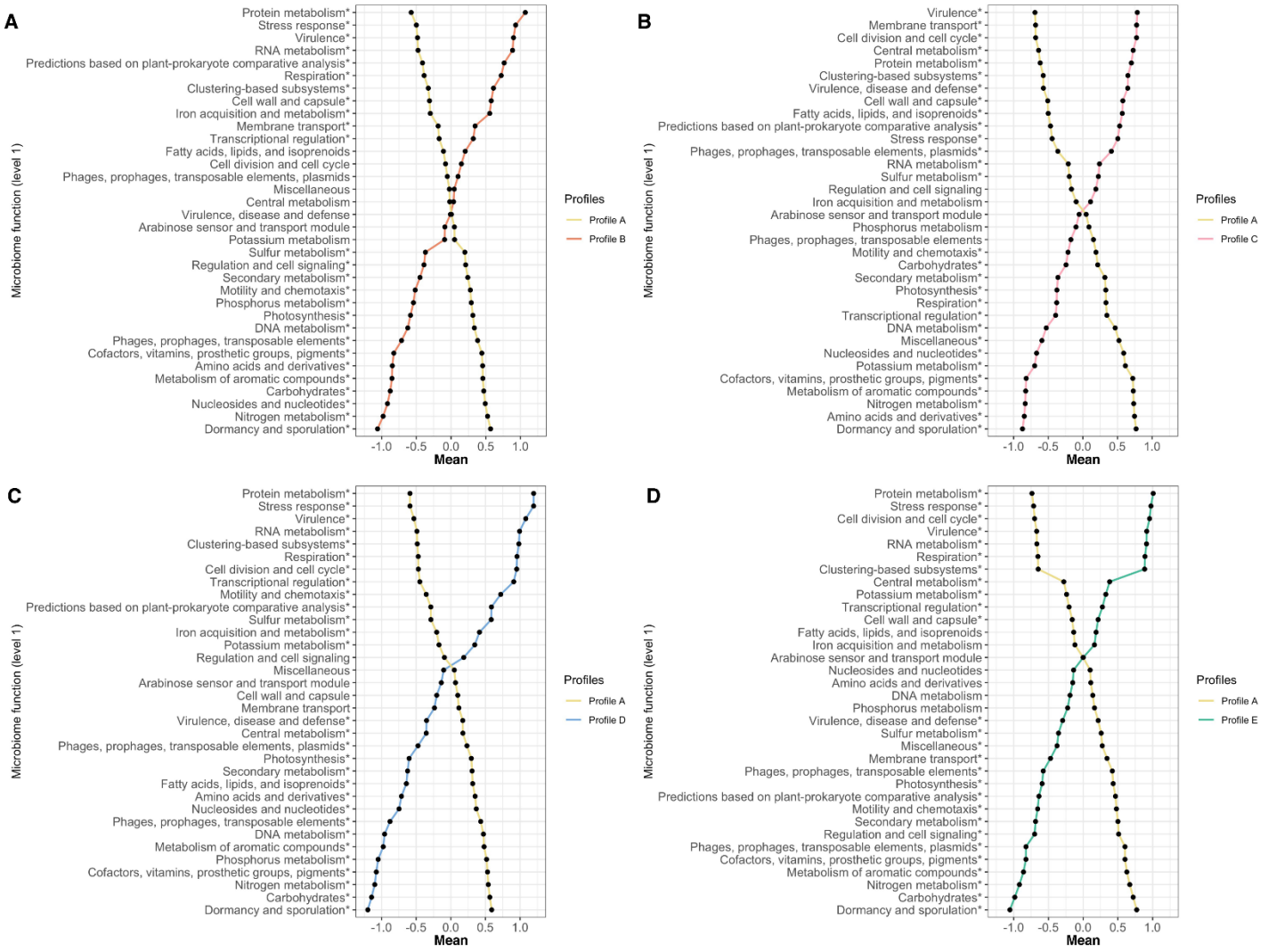

Figure 4. Between-profile differences in nasopharyngeal microbiome function among infants with bronchiolitis

In all comparisons (metatranscriptome profile A vs. each of the other profiles), the mean values of microbiome function variables (35 level-1 functions) in the corresponding profiles are plotted. The microbiome function variables are standardized by using auto-scaling after variance stabilizing transformation. The differences in more detailed microbiome functions (level-3 functions) of specific level-1 functions are presented in **Figures E8-E11**.

* False discovery rate<0.05

Abbreviations; DNA, deoxyribonucleic acid; RNA, ribonucleic acid

A. Profiles A vs. B comparison

B. Profiles A vs. C comparison

C. Profiles A vs. D comparison

D. Profiles A vs. E comparison

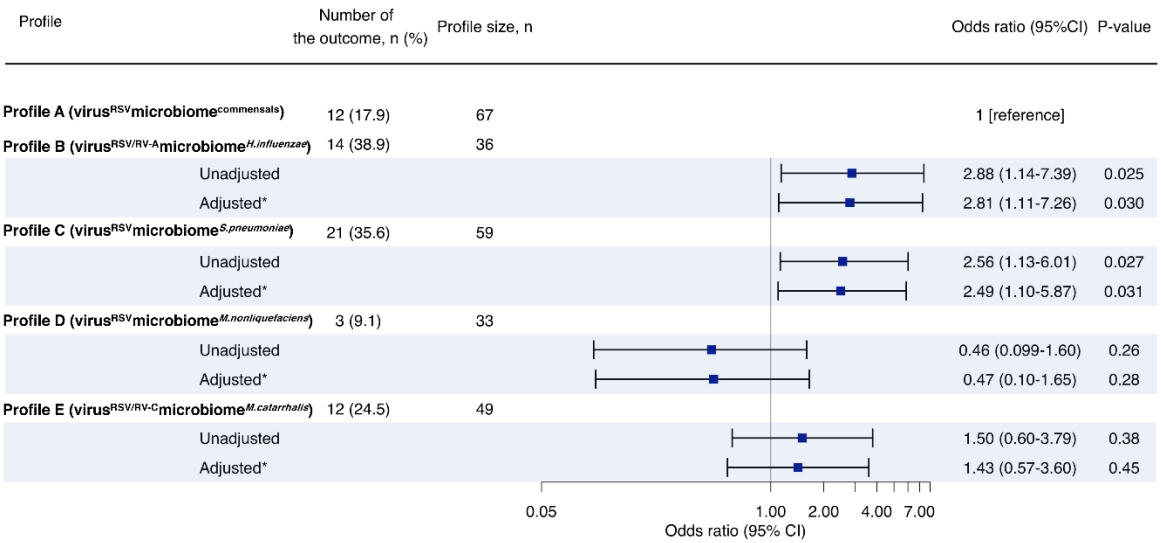

Figure 5. Association between nasopharyngeal metatranscriptome profiles of infant bronchiolitis and risk for developing asthma

Asthma (binary outcome) was defined as physician-diagnosis of asthma at age 5 years, plus either asthma medication use (e.g., albuterol inhaler, inhaled corticosteroids, montelukast) or asthma-related symptoms in the preceding year. To examine the association between bronchiolitis profiles (profile A as the reference) and the risk of developing childhood asthma, unadjusted and adjusted logistic regression models were fit.

* Multivariable random-effect logistic model adjusted for age, sex, and clustering within hospitals

Abbreviation: CI, confidence interval; RSV, respiratory syncytial virus; RV, rhinovirus

SUPPLEMENTARY MATERIALS

Nasopharyngeal metatranscriptome profiles of infants with bronchiolitis and risk of childhood asthma: a multicentre prospective study

Authors: Yoshihiko Raita, MD, MPH, MMSc; Marcos Pérez-Losada, PhD; Robert J. Freishtat, MD, MPH; Andrea Hahn, MD, MS; Eduardo Castro-Nallar, PhD; Ignacio Ramos-Tapia, PhD; Nathaniel Stearrett; Yury A. Bochkov, PhD; James E. Gern, MD; Jonathan M. Mansbach, MD, MPH, Zhaozhong Zhu, ScD; Carlos A. Camargo, Jr., MD, DrPH; and Kohei Hasegawa, MD, MPH, MS

CONTENTS

SUPPLEMENTARY METHODS

Study Design, Setting, and Participants

We analysed data from a multicentre prospective cohort study of infants hospitalized for bronchiolitis—the 35th Multicenter Airway Research Collaboration (MARC-35) study [1]. MARC-35 is coordinated by the Emergency Medicine Network (EMNet), an international research collaboration with 247 participating hospitals. At 17 sites across 14 U.S. states (**Supplementary Table S1**), MARC-35 enrolled infants (aged <1 year) who were hospitalized with an attending physician diagnosis of bronchiolitis during three bronchiolitis seasons (November 1 to April 30) from 2011 to 2014. The diagnosis of bronchiolitis was made according to the American Academy of Pediatrics bronchiolitis guidelines, defined as acute respiratory illness with a combination of rhinitis, cough, tachypnoea, wheezing, crackles, or retraction [2]. We excluded infants with a pre-existing heart and lung disease, immunodeficiency, immunosuppression, or gestational age of <32 weeks, those with a previous bronchiolitis hospitalization, or those who were transferred to a participating hospital >24 hours after initial hospitalization. All patients were treated at the discretion of the treating physicians. The institutional review board at each participating hospital approved the study with a written informed consent obtained from the parent or guardian. Of 921 infants enrolled into the longitudinal cohort, the current analysis investigated 244 infants hospitalized for bronchiolitis who were randomly selected for nasopharyngeal metatranscriptome (microbiome) and transcriptome (host) testing (**Figure 1** and **Supplementary Figure S1**).

Data Collection

Clinical data (patients' demographic characteristics, and family, environmental, and medical history, and details of the acute illness) were collected via structured interview and chart reviews. All

data were reviewed at the EMNet Coordinating Centre (Boston, MA), and site investigators were queried about missing data and discrepancies identified by manual data checks.

In addition to the clinical data, Nasopharyngeal airway samples were collected by trained site investigators using the standardized protocol that was utilized in a previous cohort study of children with bronchiolitis [1, 3]. All sites used the same collection equipment (Medline Industries, Mundelein, IL, USA) and collected the samples within 24 hours of hospitalization. The nasopharyngeal airway specimens were immediately placed on ice and then stored at −80°C. Frozen specimens were shipped in batches to Baylor College of Medicine (Houston, TX) where they were tested for 17 respiratory viruses (including respiratory syncytial virus [RSV] and rhinovirus [RV]) using real-time polymerase chain reaction (RT-PCR) assays [1, 3, 4]. For RV detection, complementary DNA was generated using virus-specific primers for RV and singleplex RT-PCR was used. The details of the RV primers and probes have been described elsewhere [5]. Next, to identify the RV species (A, B, and C), RV-positive samples were partially sequenced to determine the RV species and type at the University of Wisconsin (Madison, WI) [6]. Frozen specimens were also shipped to the University of Maryland (Baltimore, MD) for RNA sequencing (both metatranscriptome and transcriptome testing).

RNA Extraction, RNA Sequencing, and Quality Control

Total RNA was isolated from the nasopharyngeal samples using Trizol LS reagent (ThermoFisher Scientific, Waltham, MA) in combination with the Direct-zol RNA Miniprep Kit (Zymo Research, Irvine, CA). RNA quantity was measured with the Qubit 2.0 fluorometer (ThermoFisher Scientific, Waltham, MA). Its quality was assessed with the Agilent Bioanalyzer 2100 (Agilent, Palo Alto, CA) using the RNA 6000 Nano kit and we confirmed no detection of DNA contamination based on the Bioanalyzer results. Total RNA underwent DNase treatment using the TURBO DNA-free™ Kit

(ThermoFisher Scientific, Waltham, MA) for the removal of DNA contamination and underwent rRNA reduction for both human and bacterial rRNA using NEBNext rRNA Depletion Kits (New England Biolabs, Ipswich, MA). RNA was prepared for sequencing using the NEBNext Ultra II Directional RNA Library Prep Kit (New England Biolabs, Ipswich, MA) and sequenced on an Illumina NovaSeq6000 using an S4 100PE Flowcell (Illumina, San Diego, CA). All RNAseq samples had sufficient sequence depth (mean, 8,067,019 pair-end reads/sample) to obtain a high degree of sequence coverage.

Nasopharyngeal Airway Taxonomy and Function Testing

Raw sequence reads were filtered and trimmed for adapters and contaminants using the *k*-mers strategy in bbduck [7]and default settings. We used PathoScope [8] and the expanded Human Oral Microbiome Database (eHOMD) database [9] to infer bacterial taxonomy. Samples with <1,000 reads, singletons, and strains not present in at least 10% of the samples were eliminated. The metatranscriptomic analysis obtained 1,968,352,599 merged sequences and identified 323 microbial lineages after singleton removal.

Microbiome functions were estimated for bacteria and viruses separately using SUPER-FOCUS [10] and Diamond [11]and the subsystems included in the SEED database [12]. The SEED database is composed of three-level hierarchical microbiome functions: the level 1 subsystem with 35 functions, followed by the level 2 subsystem with 194 functions, and the level 3 subsystem with 1,290 functions. All the analyses were carried out in the high-performance computing cluster PEGASUS at the George Washington University (DC, USA).

Nasopharyngeal Airway Host Transcriptome

Transcript abundances from clean RNAseq reads were estimated in Salmon [13]using the human transcriptome (hg38) and the mapping-based mode. We first generated a decoy-aware transcriptome and then quantified the reads using Salmon's default settings and the following flags: –validateMappings, –recoverOrphans, –seqBias and –gcBias. Salmon is fast and accurate, corrects for potential changes in gene length across samples (e.g., from differential isoform usage), and has great sensitivity.

Functional and Clinical Outcomes

The outcomes of interest are a) host function (the nasopharyngeal transcriptome) at index hospitalization for bronchiolitis and b) asthma development by age 5 years. The definition of asthma was based on a commonly-used epidemiologic definition of asthma [14, 15]—physician-diagnosis of asthma by age 5 years, plus either asthma medication use (e.g., albuterol inhaler, inhaled corticosteroids, montelukast) or asthma-related symptoms in the preceding year.

Statistical Analysis

The objectives of the current study are a) to identify biologically distinct metatranscriptome profiles among infants with bronchiolitis and b) to relate them to biologically meaningful pathways of the transcriptome and risks of asthma development. The analytic workflow is summarized in **Figure 1**.

First, we preprocessed variables with appropriate variance stabilization methods and computed a distance matrix for each of three datasets—1) virus, 2) microbiome taxonomy (species-level), and 3) microbiome function data. For the virus data, we used the viral genomic load for RSV, RV-A, and RV-C

given their importance in bronchiolitis and asthma [16]. For the microbiome taxonomy data, we used the relative abundance of the 40 most abundant species, which accounted for 95% of the total abundance. For the microbiome function data, we selected level-2 functions with high variances (median absolute deviation >0.75) with variance stabilizing transformation using *DESeq2* package [17].Then, we computed Euclidean distance for the virus data using *amap* package [18], Bray-Curtis distance for the taxonomy data using *vegan* package [19], and Pearson distance for the microbiome function data using *amap* package [18].

To conduct metatranscriptome profiling (or clustering), we computed an affinity matrix of each dataset separately and computed a fused affinity matrix by similarity network [20]fusion using *SNFtool* package [21]. We set all parameters of similarity network fusion (i.e., the number of neighbours [n=25], hyperparameter [alpha=0.7], and the number of iteration [T=25]) based on a grid search by computing network modularity. Finally, to identify mutually exclusive metatranscriptome profiles (or clusters), we applied spectral clustering to the fused affinity matrix [20]. To determine an optimal number of profiles, we used a combination of the silhouette scores (**Supplementary Figure S2, Panel A**), network modularity (**Supplementary Figure S2, Panel B**), profile size (n=33-67), and clinical and biological plausibility [1, 15, 16]. The network modularity measures how well-separated subnetworks are given a particular partitioning (i.e., profiles) of the network [22].To test the stability of profiles as internal validation, we conducted a label propagation method using leave-one-out cross-validation and 5-fold cross-validation with 100 iterations (**Supplementary Figure S3**). We also computed the ranking of normalized mutual information (NMI) score of each variable. Each variable is ranked based on the similarity in the clustering of the fused matrix, meaning that high-ranked variables contribute more to form the similarity network. After deriving the metatranscriptome profiles, we applied the t-distributed stochastic neighbour embedding (t-sne) method to the five eigenvectors in the spectral clustering for the

visualization of the profiles. We also visualized a patient similarity network with Fruchterman-Reingold layout using *qgraph* package [23].

Additionally, we conducted several analyses to examine the between-profile differences in the virus genomic load, taxonomy, and functional data. First, we examined the differences in the patient characteristics and clinical presentation by using Kruskal-Wallis, chi-squared, and Fisher exact tests, as appropriate. Second, to examine the relationship between the profiles and major clinical variables, we developed chord diagrams, a Venn diagram of three major clinical variables (parental asthma, parental eczema, and IgE sensitization) and their intersections, and an upset plot corresponding to the presented Venn diagram. We used *circlize* package [24] for the chord diagram, *VennDiagram* package [25] for the Venn diagram, and *ComplexUpset* package [26] for the upset plot. Third, to visualize the between-profile differences in the viruses and selected microbiome species, we developed a heatmap assigning the mean value for the virus and taxonomy data. The viral genomic load data are treated as numeric variables and processed by auto-scaling. The taxonomy data (30 most abundant species) are processed by $\log_2$ transformation and auto-scaling. We also developed pirate plots (a combination of a violin plot and a box plot) for the taxonomy data. Fourth, to visualize the between-profiles differences in the microbiome function (level 1 functions) by comparing the reference profile (profile A) with each of the other four profiles, we developed ranked plots using the mean standardized difference between the profile pairs. Lastly, to visualize the differences in more-detailed microbiome functions (level 3 functions) of specific level 1 function of interest, we also developed additional ranked plots.

After deriving the metatranscriptome profiles, we examined their relationship with host transcriptome and the longitudinal relationship with asthma development by age 5 years (**Figure 1**). For transcriptome data, we conducted differential gene expression analysis and functional pathway analysis by comparing the reference profile (profile A) with each of the other four profiles. To investigate

whether genes for specific biological pathways are enriched among the large positive or negative fold changes, we conducted a functional class scoring analysis using *clusterProfiler* package [27]. To determine the association of profiles with the risk of childhood asthma (binary outcome), we fit unadjusted and adjusted logistic regression models accounting for patient clustering within sites.
In the sensitivity analysis that examines the robustness of profile-outcome associations, we also repeated the analysis using a different number of profiles. We analysed the data using R version 3.6.1 (R Foundation for Statistical Computing, Vienna, Austria). All P-values were two-tailed, with $P<0.05$ considered statistically significant. We corrected for multiple testing using the Benjamini-Hochberg FDR method [28].

SUPPLEMENTARY REFERENCES

1. Hasegawa K, Mansbach JM, Ajami NJ et al. Association of nasopharyngeal microbiota profiles with bronchiolitis severity in infants hospitalised for bronchiolitis. Eur Respir J 2016;48(5):1329-1339.
2. Ralston SL, Lieberthal AS, Meissner HC et al. Clinical practice guideline: The diagnosis, management, and prevention of bronchiolitis. Pediatrics 2014;134(5):e1474-e1502.
3. Hasegawa K, Jartti T, Mansbach JM et al. Respiratory syncytial virus genomic load and disease severity among children hospitalized with bronchiolitis: Multicenter cohort studies in the United States and Finland. J Infect Dis 2015;211(10):1550-1559.
4. Mansbach JM, Piedra PA, Stevenson MD et al. Prospective multicenter study of children with bronchiolitis requiring mechanical ventilation. Pediatrics 2012;130(3):e492-e500.
5. Lu X, Holloway B, Dare RK, Kuypers J et al. Real-time reverse transcription-PCR assay for comprehensive detection of human rhinoviruses. J Clin Microbiol 2008;46(2):533-539.
6. Bochkov YA, Grindle K, Vang F et al. Improved molecular typing assay for rhinovirus species A, B, and C. J Clin Microbiol 2014; 52: 2461–2471
7. BBMap download | SourceForge.net [Internet]. [cited 2021 Apr 2]. Available from: https://sourceforge.net/projects/bbmap/.
8. Hong C, Manimaran S, Shen Y et al. PathoScope 2.0: A complete computational framework for strain identification in environmental or clinical sequencing samples. Microbiome 2014; 2:33
9. Escapa IF, Chen T, Huang Y et al. New Insights into Human Nostril Microbiome from the Expanded Human Oral Microbiome Database (eHOMD): a Resource for the Microbiome of the Human Aerodigestive Tract. mSystems 2018;3(6):e00187-18.

10. Silva GGZ, Green KT, Dutilh BE et al. SUPER-FOCUS: A tool for agile functional analysis of shotgun metagenomic data. Bioinformatics 2016; 32: 354–361
11. Buchfink B, Xie C, Huson DH. Fast and sensitive protein alignment using DIAMOND. Nat Methods 2015;12(1):59-60.
12. Overbeek R, Dlsz T, Stevens R. The seed: A peer-to-peer environment for genome annotation. Communications of the ACM 2004; 46–50
13. Patro R, Duggal G, Love MI, Irizarry RA, Kingsford C. Salmon provides fast and bias-aware quantification of transcript expression. Nat Methods 2017; 14: 417–419
14. Camargo CA, Ingham T, Wickens K et al. Cord-blood 25-hydroxyvitamin D levels and risk of respiratory infection, wheezing, and asthma. Pediatrics 2011;127(1):e180-e187.
15. Raita Y, Camargo CA, Bochkov YA et al. Integrated-omics endotyping of infants with rhinovirus bronchiolitis and risk of childhood asthma. J Allergy Clin Immunol 2021;147(6):2108-2117.
16. Hasegawa K, Dumas O, Hartert T et al. Advancing our understanding of infant bronchiolitis through phenotyping and endotyping: clinical and molecular approaches. Expert Rev Respir Med 2016;10(8):891-899.
17. Love MI, Huber W, Anders S. Moderated estimation of fold change and dispersion for RNA-seq data with DESeq2. *Genome Biology* 2014;15(12):550
18. CRAN - Package amap [Internet]. [cited 2021 Apr 2]. Available from: https://cran.r-project.org/web/packages/amap/index.html.
19. CRAN - Package vegan [Internet]. [cited 2021 Apr 2]. Available from: https://cran.r-project.org/web/packages/vegan/index.html.

20. Wang B, Mezlini AM, Demir F, Fiume M, Tu Z, Brudno M, Haibe-Kains B, Goldenberg A. Similarity network fusion for aggregating data types on a genomic scale. Nat Methods 2014;11(3):333–337

21. CRAN - Package SNFtool [Internet]. [cited 2021 Apr 2]. Available from: https://cran.r-project.org/web/packages/SNFtool/index.html.

22. Newman MEJ. Modularity and community structure in networks. Proc Natl Acad Sci; 2006; 103: 8577–8582

23. Epskamp S, Cramer AOJ, Waldorp LJ et al: Network visualizations of relationships in psychometric data. *Journal of Statistical Software* [Internet] American Statistical Association; 2012 [cited 2021 Apr 2]; 48: 1–18 Available from: https://www.jstatsoft.org/index.php/jss/article/view/v048i04/v48i04.pdf.

24. CRAN - Package circlize [Internet]. [cited 2021 Apr 2]. Available from: https://cran.r-project.org/web/packages/circlize/index.html.

25. CRAN - Package VennDiagram [Internet]. [cited 2021 Apr 2]. Available from: https://cran.r-project.org/web/packages/VennDiagram/.

26. CRAN - Package ComplexUpset [Internet]. [cited 2021 Apr 2]. Available from: https://cran.r-project.org/web/packages/ComplexUpset/index.html.

27. Yu G, Wang LG, Han Y et al. ClusterProfiler: An R package for comparing biological themes among gene clusters. OMICS 2012;16(5):284-287.

28. Benjamini Y, Hochberg Y. Controlling the False Discovery Rate: A Practical and Powerful Approach to Multiple Testing. *Journal of the Royal Statistical Society* 1995; 57: 289–300

Supplementary Table S1. Principal investigators at the 17 participating sites in MARC-35

Amy D. Thompson, MD	Alfred I. duPont Hospital for Children, Wilmington, DE
Federico R. Laham, MD, MS	Arnold Palmer Hospital for Children, Orlando, FL
Jonathan M. Mansbach, MD, MPH	Boston Children's Hospital, Boston, MA
Vincent J. Wang, MD, MHA and Susan Wu, MD	Children's Hospital of Los Angeles, Los Angeles, CA
Michelle B. Dunn, MD and Jonathan M. Spergel, MD, PhD	Children's Hospital of Philadelphia, Philadelphia, PA
Juan C. Celedón, MD, DrPH	Children's Hospital of Pittsburgh, Pittsburgh, PA
Michael R. Gomez, MD, MS-HCA and Nancy Inhofe, MD	The Children's Hospital at St. Francis, Tulsa, OK
Brian M. Pate, MD and Henry T. Puls, MD	The Children's Mercy Hospital & Clinics, Kansas City, MO
Stephen J. Teach, MD, MPH	Children's National Medical Center, Washington, D.C.
Richard T. Strait, MD and Stephen C. Porter, MD, MSc, MPH	Cincinnati Children's Hospital and Medical Center, Cincinnati, OH
Ilana Y. Waynik, MD	Connecticut Children's Medical Center, Hartford, CT
Sujit Iyer, MD	Dell Children's Medical Center of Central Texas, Austin, TX
Michelle D. Stevenson, MD, MS	Norton Children's Hospital, Louisville, KY
Margaret Samuels-Kalow, MD, MPhil, Wayne G. Shreffler, MD, PhD and Ari R. Cohen, MD	Massachusetts General Hospital, Boston, MA
Anne K. Beasley, MD and Cindy S. Bauer, MD	Phoenix Children's Hospital, Phoenix, AZ
Thida Ong, MD and Markus Boos, MD, PhD	Seattle Children's Hospital, Seattle, WA
Charles G. Macias, MD, MPH	Texas Children's Hospital, Houston, TX

Supplementary Table S2. Comparisons between analytic and non-analytic cohorts in infants with bronchiolitis in the MARC-35 cohort

Characteristics	Analytic cohort (n=244)	Non-analytic cohort (n=677)	P-value
Demographics			
Age (month), median (IQR)	3 (2–6)	3 (2–6)	0.85
Female sex	98 (40.2)	269 (39.7)	0.97
Race/ethnicity			0.93
Non-Hispanic white	102 (41.8)	299 (44.2)	
Non-Hispanic black	57 (23.4)	153 (22.6)	
Hispanic	76 (31.1)	199 (29.4)	
Other or unknown	9 (3.7)	26 (3.8)	
Prematurity (32–36.9 weeks)	47 (19.3)	124 (18.3)	0.48
Birth weight (kg), median (IQR)	3.20 (2.89–3.57)	3.29 (2.90–3.60)	0.28
Mode of birth (caesarean delivery)	84 (35.0)	228 (34.1)	0.86
Previous breathing problems (count)			0.19
0	204 (83.6)	530 (78.3)	
1	30 (12.3)	116 (17.1)	
2	10 (4.1)	31 (4.6)	
Previous ICU admission	4 (1.6)	11 (1.6)	0.99
History of eczema	31 (12.7)	106 (15.7)	0.31
Lifetime antibiotic use	79 (32.4)	216 (31.9)	0.96
Ever attended daycare	71 (29.1)	140 (20.7)	0.01
Cigarette smoke exposure at home	34 (13.9)	104 (15.4)	0.67
Maternal smoking during pregnancy	34 (14.2)	92 (13.8)	0.96
Parental history of asthma	76 (31.1)	229 (33.9)	0.48
Parental history of eczema	46 (18.9)	129 (19.1)	0.99
Clinical presentation			
Weight at presentation (kg), median (IQR)	6.07 (4.60–7.99)	6.10 (4.80–7.60)	0.98
Respiratory rate at presentation (per minute), median (IQR)	48 (40–60)	49 (40–60)	0.72
Oxygen saturation at presentation			0.16
<90%	29 (12.2)	106 (16.0)	
90–93%	190 (80.2)	491 (73.9)	
≥94%	18 (7.6)	67 (10.1)	
Blood eosinophilia (≥4%)	21 (10.1)	61 (10.3)	0.99
IgE sensitization (%)	51 (20.9)	131 (19.4)	0.67
Respiratory virus			
RSV infection	222 (91.0)	530 (78.3)	<0.001
Solo-RSV infection	159 (65.2)	383 (56.4)	0.021
RV infection			
RV-A	26 (10.7)	62 (9.2)	0.58
RV-B	4 (1.6)	11 (1.6)	0.99
RV-C	21 (8.6)	61 (9.0)	0.95
Solo-RV infection	13 (5.3)	39 (5.8)	0.93
RSV/RV coinfection	29 (11.9)	80 (11.8)	0.99

Abbreviations: IQR, interquartile range; ICU, intensive care unit; IgE, immunoglobulin E; RSV, respiratory syncytial virus; RV, rhinovirus

Data are no. (%) of infants unless otherwise indicated. Percentages may not equal 100, because of rounding and missingness.

Supplementary Table S3. Sensitivity analysis using four metatranscriptome profiles

	Profile 1 (n=69)	Profile 2 (n=78)	Profile 3 (n=44)	Profile 4 (n=53)	P-value	FDR
Original 5 profiles (A-E)						
Profile A (n=67): virus^{RSV}microbiome^{commensals}	65 (94.2)	2 (2.6)	0 (0.0)	0 (0.0)		
Profile B (n=36): virus$^{RSV/RV-A}$microbiome$^{H.influenzae}$	0 (0.0)	30 (38.5)	5 (11.4)	1 (1.9)		
Profile C (n=59): virus^{RSV}microbiome$^{S.pneumoniae}$	4 (5.8)	46 (59.0)	6 (13.6)	3 (5.7)		
Profile D (n=33): virus^{RSV}microbiome$^{M.nonliquefaciens}$	0 (0.0)	0 (0.0)	33 (75.0)	0 (0.0)		
Profile E (n=49): virus$^{RSV/RV-C}$microbiome$^{M.catarrhalis}$	0 (0.0)	0 (0.0)	0 (0.0)	49 (92.5)		
Demographics						
Age (month), median (IQR)	3 (1-6)	3 (2-6)	4 (2-7)	3 (2-5)	0.44	
Female sex	30 (43.5)	30 (38.5)	18 (40.9)	20 (37.7)	0.91	
Race/ethnicity					0.52	
Non-Hispanic white	30 (43.5)	27 (34.6)	19 (43.2)	26 (49.1)		
Non-Hispanic black	14 (20.3)	22 (28.2)	11 (25.0)	10 (18.9)		
Hispanic	23 (33.3)	26 (33.3)	14 (31.8)	13 (24.5)		
Other or unknown	2 (2.9)	3 (3.8)	0 (0.0)	4 (7.5)		
Prematurity (32–36.9 weeks)	15 (21.7)	16 (20.5)	10 (22.7)	6 (11.3)	0.42	
Birth weight (kg), median (IQR)	3.20 (2.90-3.52)	3.30 (2.84-3.60)	3.09 (2.80-3.39)	3.31 (3.01-3.62)	0.50	
Mode of birth (caesarean delivery)	18 (26.5)	33 (42.9)	15 (34.1)	18 (35.3)	0.23	
Previous breathing problems (count)					0.96	
0	58 (84.1)	65 (83.3)	36 (81.8)	45 (84.9)		
1	8 (11.6)	10 (12.8)	5 (11.4)	7 (13.2)		
2	3 (4.3)	3 (3.8)	3 (6.8)	1 (1.9)		
Previous ICU admission	3 (4.3)	0 (0.0)	1 (2.3)	0 (0.0)	0.11	
History of eczema	3 (4.3)	15 (19.2)	4 (9.1)	9 (17.0)	0.026	
Lifetime antibiotic use*	26 (37.7)	28 (35.9)	7 (15.9)	18 (34.0)	0.063	
Ever attended daycare	15 (21.7)	24 (30.8)	15 (34.1)	17 (32.1)	0.44	
Cigarette smoke exposure at home	9 (13.0)	13 (16.7)	8 (18.2)	4 (7.5)	0.37	
Maternal smoking during pregnancy	9 (13.2)	14 (18.2)	3 (6.8)	8 (15.7)	0.37	
Parental history of asthma	15 (21.7)	28 (35.9)	17 (38.6)	16 (30.2)	0.18	
Parental history of eczema	9 (13.0)	18 (23.1)	13 (29.5)	6 (11.3)	0.056	
Clinical Presentation						
Weight at presentation (kg), median (IQR)	5.50 (4.35-7.35)	6.35 (4.93-7.48)	6.75 (5.05-8.25)	6.20 (4.80-7.92)	0.24	

Respiratory rate at presentation (per minute), median (IQR)	48 (40-55)	48 (38-60)	51 (44-63)	52 (41-60)	0.19	
Oxygen saturation at presentation					0.33	
<90%	12 (18.5)	8 (10.5)	2 (4.7)	7 (13.2)		
90-93%	49 (75.4)	62 (81.6)	39 (90.7)	40 (75.5)		
≥94%	4 (6.2)	6 (7.9)	2 (4.7)	6 (11.3)		
Blood eosinophilia (≥4%)	4 (6.9)	6 (9.0)	3 (7.9)	8 (17.8)	0.30	
IgE sensitization	11 (15.9)	17 (21.8)	11 (25.0)	12 (22.6)	0.64	
Clinical course						
Positive pressure ventilation use†	6 (8.7)	7 (9.0)	3 (6.8)	2 (3.8)	0.70	
Intensive treatment use‡	12 (17.4)	16 (20.5)	3 (6.8)	11 (20.8)	0.19	
Length of day (day), median (IQR)	2 (1-3)	2 (1-4)	2 (1-3)	2 (1-3)	0.76	
Antibiotic use during hospitalization	27 (39.1)	31 (39.7)	9 (20.5)	13 (24.5)	0.054	
Corticosteroid use during hospitalization	9 (13.0)	13 (16.7)	3 (6.8)	4 (7.5)	0.32	
Respiratory virus						
RSV solo infection	45 (65.2)	56 (71.8)	31 (70.5)	27 (50.9)	0.079	
Rhinovirus coinfection	5 (7.2)	8 (10.3)	5 (11.4)	11 (20.8)	0.16	
Rhinovirus-A	7 (10.1)	11 (14.1)	4 (9.1)	4 (7.5)	0.70	
Rhinovirus-B	1 (1.4)	1 (1.3)	1 (2.3)	1 (1.9)	0.99	
Rhinovirus-C	2 (2.9)	0 (0.0)	2 (4.5)	17 (32.1)	<0.001	
Chronic comorbidities						
Asthma at age 5 years	13 (18.8)	27 (34.6)	10 (22.7)	12 (22.6)	0.16	
Microbiome relative abundance§, median (IQR)						
Streptococcus pneumoniae	0.22 (0.12-0.39)	0.20 (0.07-0.61)	0.05 (0.02-0.33)	0.06 (0.01-0.24)	<0.001	<0.001
Moraxella catarrhalis	0.00 (0.00-0.04)	0.01 (0.00-0.06)	0.05 (0.01-0.18)	0.65 (0.48-0.88)	<0.001	<0.001
Moraxella nonliquefaciens	0.00 (0.00-0.00)	0.00 (0.00-0.03)	0.57 (0.01-0.74)	0.00 (0.00-0.03)	<0.001	<0.001
Cutibacterium acnes	0.22 (0.12-0.36)	0.01 (0.00-0.07)	0.01 (0.00-0.02)	0.01 (0.00-0.02)	<0.001	<0.001
Haemophilus influenzae	0.00 (0.00-0.01)	0.01 (0.00-0.34)	0.00 (0.00-0.01)	0.00 (0.00-0.01)	<0.001	<0.001

* Any systemic antibiotic use from birth up to the index hospitalization for bronchiolitis.

† Infants with bronchiolitis who underwent continuous positive airway ventilation and/or mechanical ventilation.

‡ Infants with bronchiolitis who were admitted to ICU and/or who underwent positive pressure ventilation.

§ For microbiome taxonomy data, the five most abundant species are presented.

Abbreviations: IQR, interquartile range; ICU, intensive care unit; IgE, immunoglobulin E; RSV, respiratory syncytial virus; RV-A, rhinovirus A; RV-C, rhinovirus C

Supplementary Figure S1. Study flow diagram

The differences in the analytic and non-analytic cohorts are summarized in **Table E1**.
* The metatranscriptome and transcriptome data are obtained in 244 infants who were *randomly* selected from the longitudinal cohort.

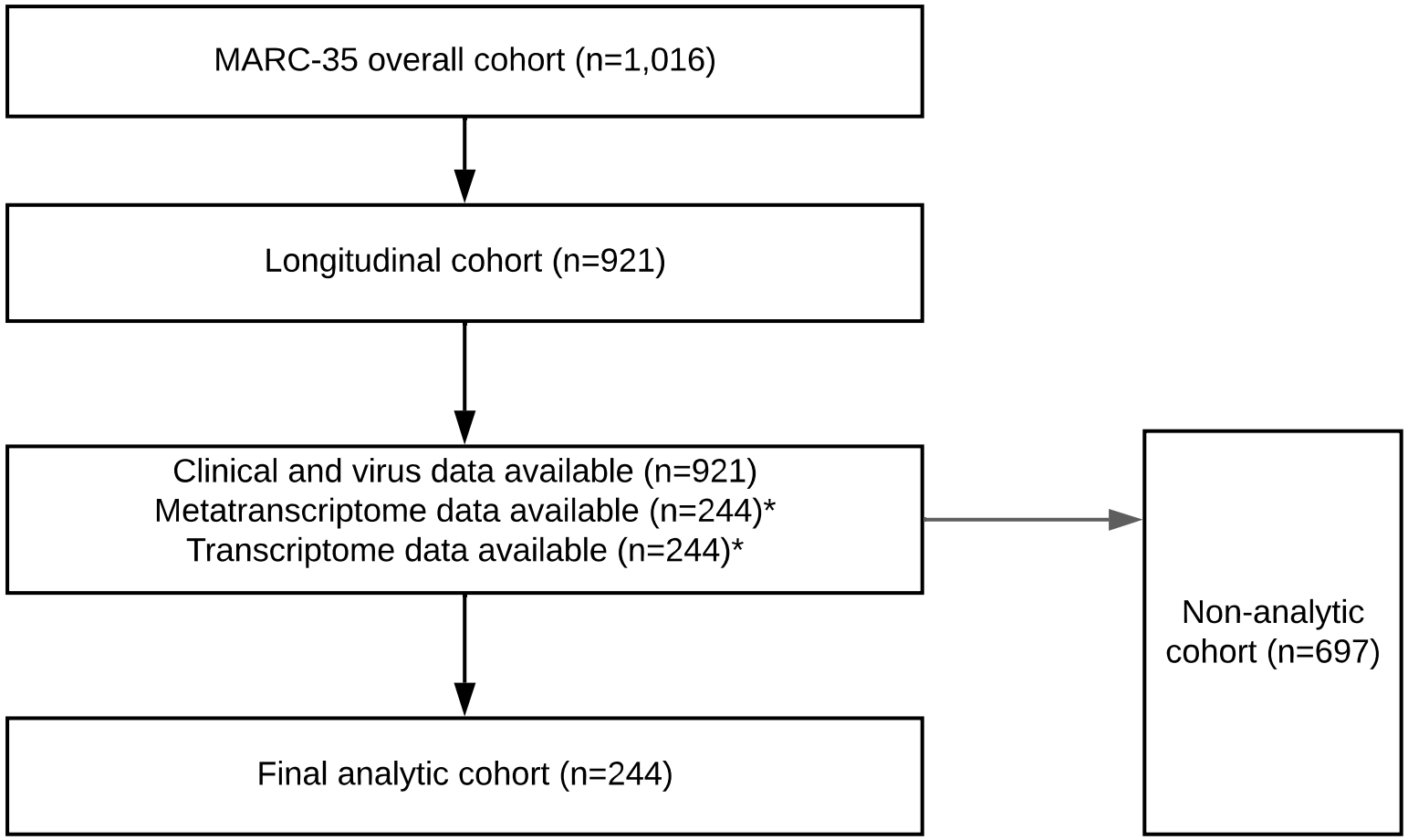

Supplementary Figure S1. Average silhouette score and network modularity, according to number of metatranscriptome profiles

A. Average silhouette score, according to number of metatranscriptome profiles
Across the different numbers of profiles (*k* of 3-7), the average silhouette score was highest with *k*=5.

B. **Network modularity, according to number of metatranscriptome profiles**
Across the different numbers of profiles (*k* of 2-10), the network modularity was highest with *k*=5.

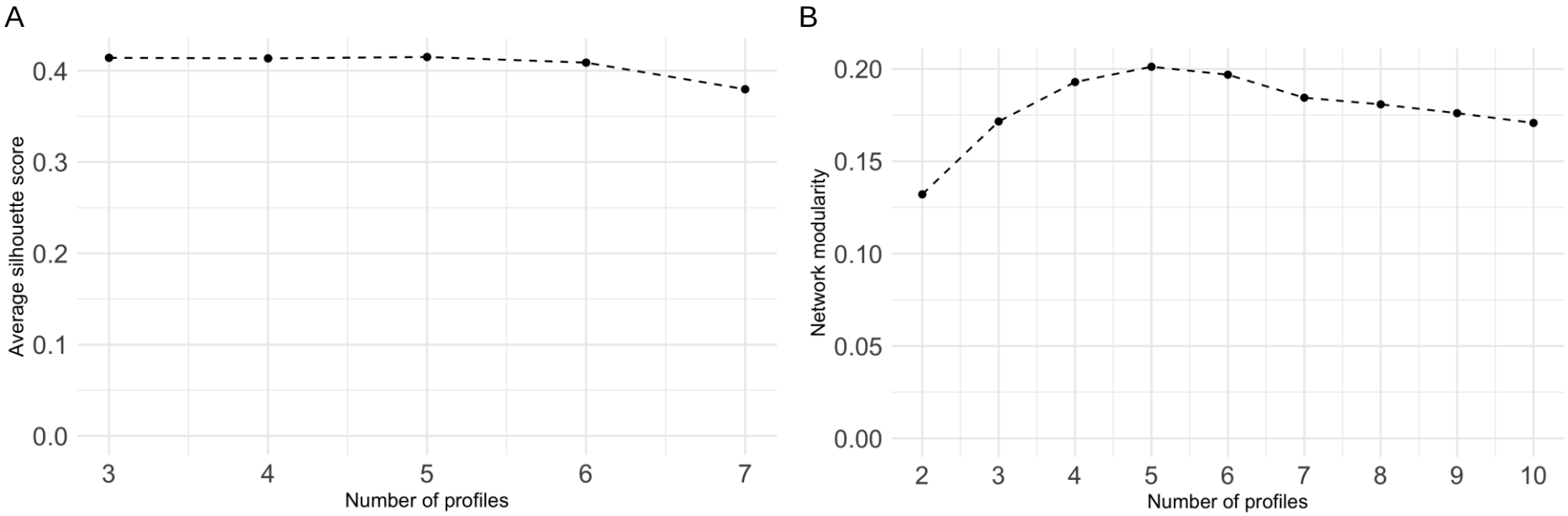

Supplementary Figure S3. Accuracy of metatranscriptome profiles using label propagation methods, according to number of profiles

A. Accuracy using leave-one-out cross-validation, according to number of metatranscriptome profiles
Across the different numbers of profiles (*k* of 3-7), the accuracy was highest with *k*=5.

B. **Accuracy using 5-fold cross-validation, according to number of metatranscriptome profiles**
Across the different numbers of profiles (*k* of 3-7), the accuracy was highest with *k*=5.

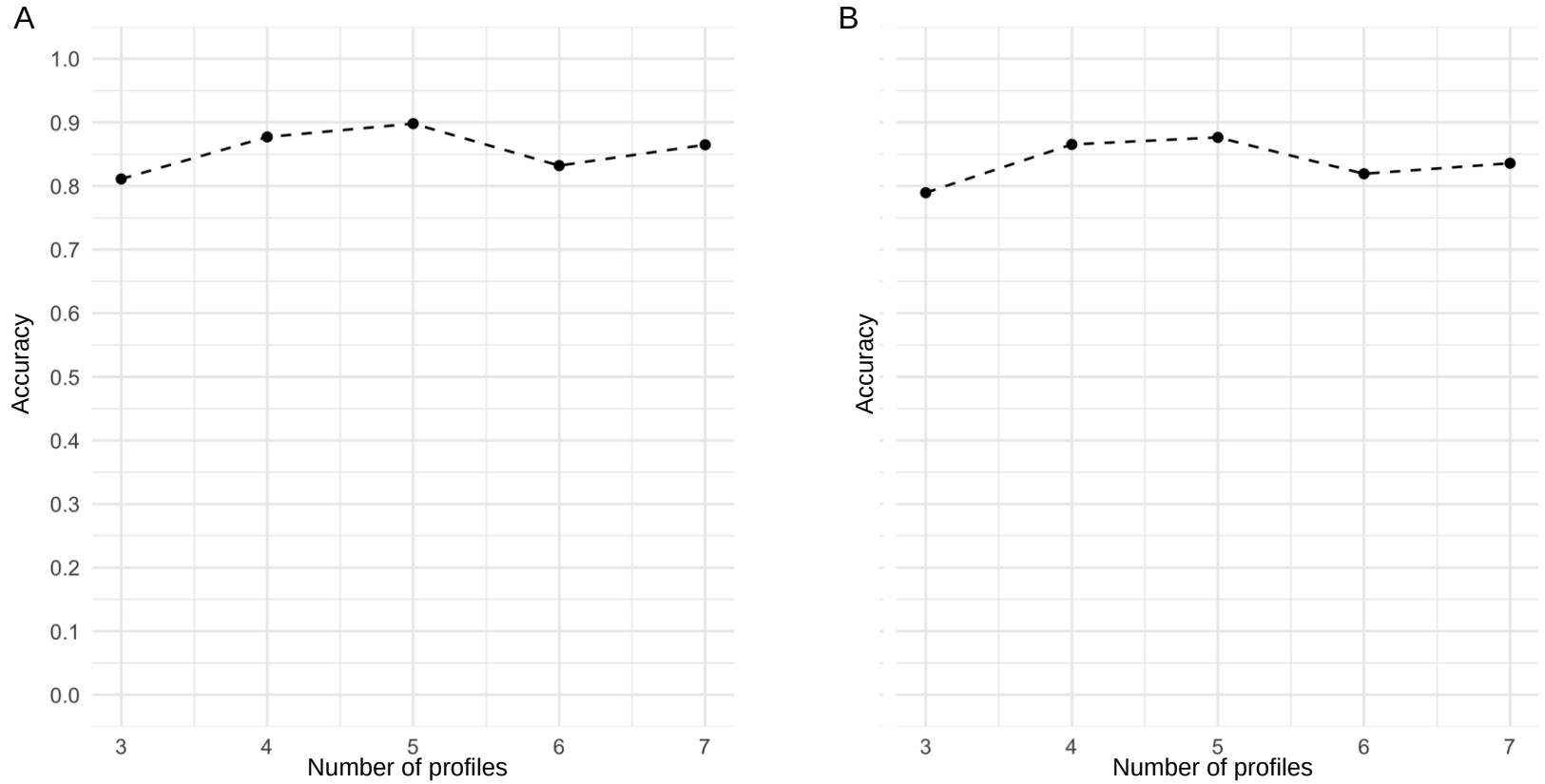

Supplementary Figure S4. Similarity network visualization of metatranscriptome profiles among infants with bronchiolitis
The goal of this figure is a network visualization. We applied integrative network and clustering approaches to the virus, nasopharyngeal microbiome taxonomy, and microbiome function data. This network-based clustering method identifies distinct profiles based on the degree of connectivity. In other words, infants with similar biological characteristics are more closely connected with each other based on the degree of biological similarity (**Figure 1**), resulting in the formation of a connected component (i.e., a profile) in the network.

Nodes (circles) with the same colour represent infants with a corresponding profile (A, B, C, D, and E). Network graphs in the integrated omics similarity network are visualized using with Fruchterman-Reingold layout. The layout of the network from the three datasets is fixed with the position of the integrated omics similarity network. We selected 1,500 edges with the highest similarity for the network visualization and the width of the edge reflects the strength of similarity.
Abbreviations: RSV, respiratory syncytial virus; RV-A, rhinovirus A; RV-C, rhinovirus C

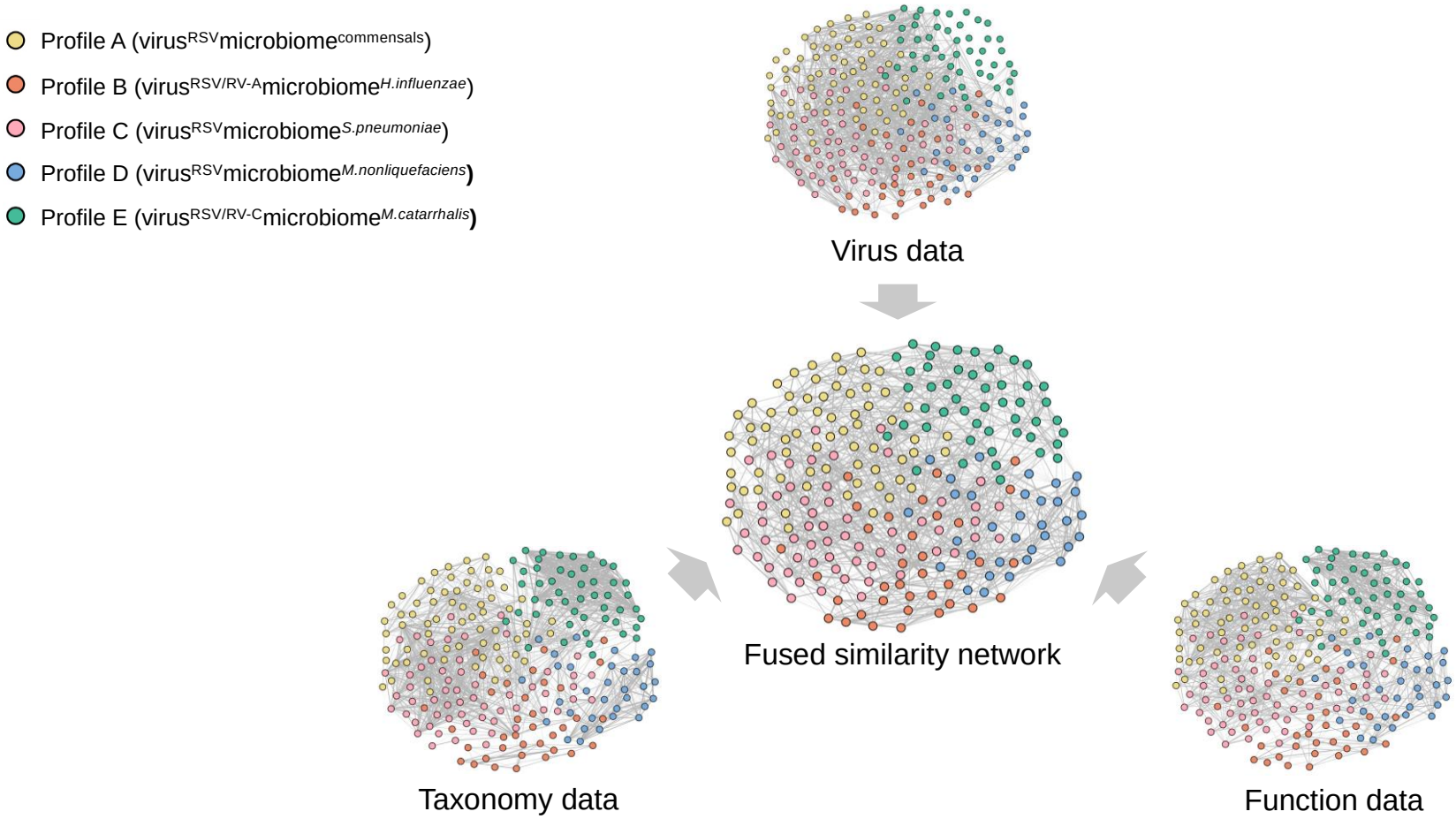
Profile A (virus^RSV microbiome^commensals)
Profile B (virus^RSV/RV-A microbiome^H.influenzae)
Profile C (virus^RSV microbiome^S.pneumoniae)
Profile D (virus^RSV microbiome^M.nonliquefaciens)
Profile E (virus^RSV/RV-C microbiome^M.catarrhalis)
Virus data
Fused similarity network
Taxonomy data
Function data

Supplementary Figure S5. Major clinical and virus characteristics according to metatranscriptome profiles

The y-axis of the bar plots represents the proportion of infants within the profile who have the corresponding clinical or virus characteristic, which was scaled to a total of 100%. For example, the profile B infants (light orange) had a high proportion of lifetime antibiotics use, history of eczema, parental eczema, IgE sensitization, blood eosinophilia, and coinfection with RV-A. Profile C (pink) infants had a high proportion of parental asthma and solo-RSV infection.

Abbreviations: IgE, immunoglobulin E; RSV, respiratory syncytial virus; RV, rhinovirus; RV-A, rhinovirus A; RV-C, rhinovirus C

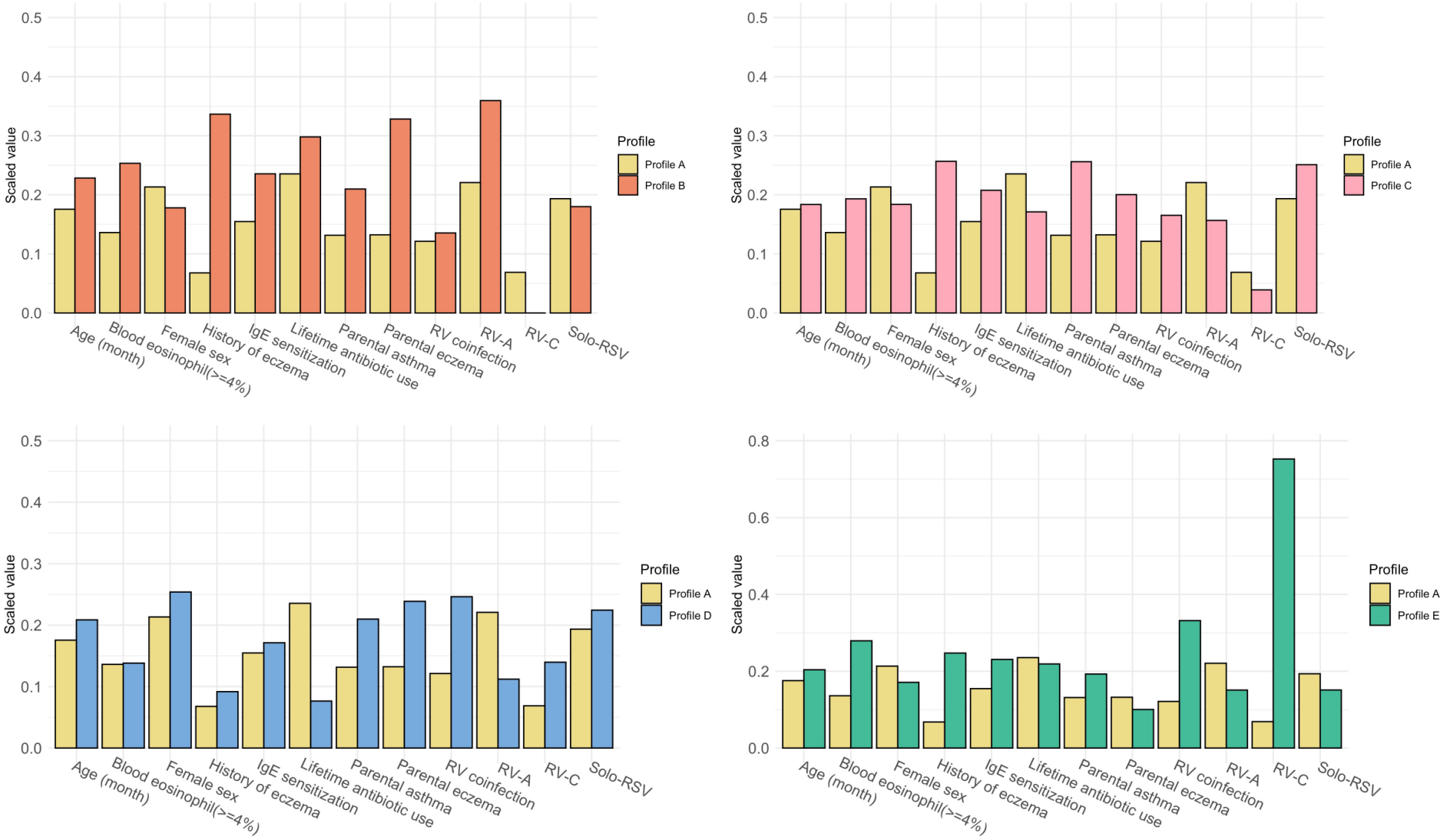

Supplementary Figure S6. Relationship between metatranscriptome profiles and major clinical variables

A. Venn diagram of three major clinical variables (parental asthma, parental eczema, and IgE sensitization) and their intersections
The Venn diagram illustrates the composition of three major clinical variables and their intersections. The numbers correspond to the number of infants in each subset and intersection

B. Upset plot, corresponding to the presented Venn diagram
The plot illustrates the composition of three major clinical variables and their intersections visualized based on the five metatranscriptome profiles. Vertical stacked bar charts reflect the number of infants within each subset and intersection coloured according to the profiles. Horizontal bars indicate the number of infants in each clinical variable set. Black dots indicate the sets of subsets and intersections; connecting lines indicate relevant intersections related to each stacked bar chart.
Abbreviation: IgE, immunoglobulin E

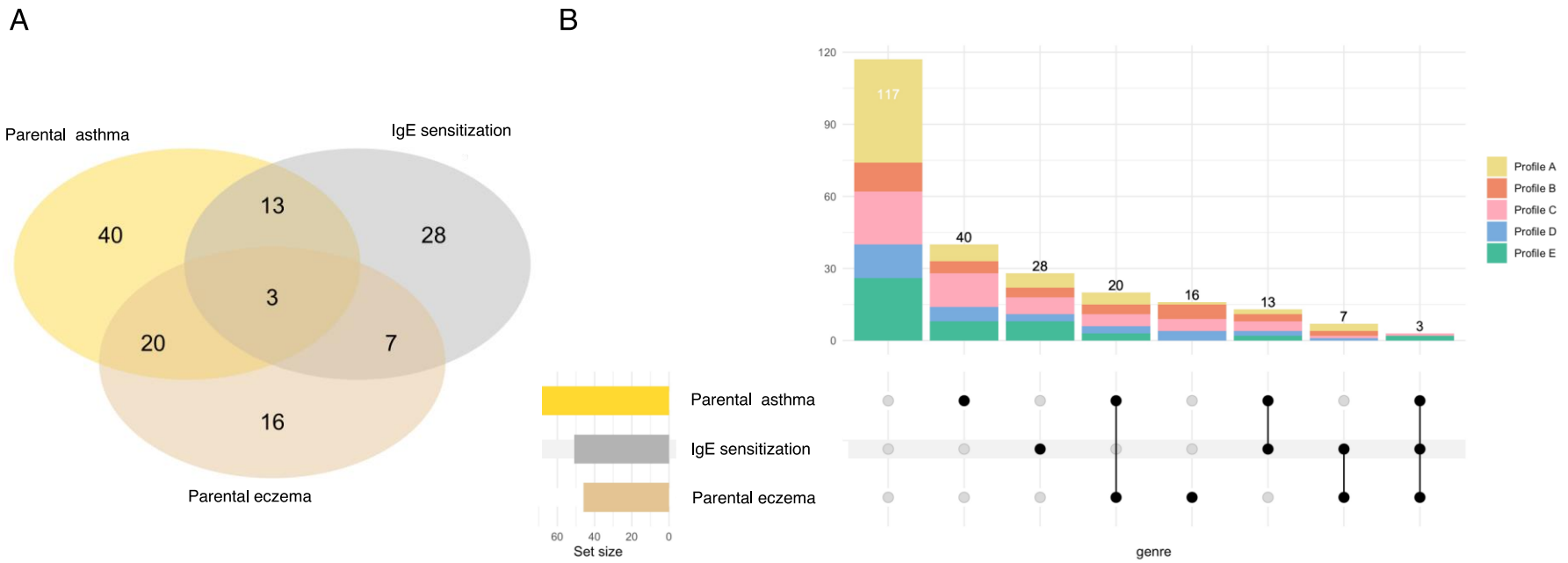

Supplementary Figure S7. Between-profile differences in clinical variables, virus, and nasopharyngeal microbiome (taxonomy) in infants with bronchiolitis

To visualize the between-profile differences, the clinical variables and viruses are treated as numeric variables and processed by auto-scaling. The microbiome taxonomy data (30 most abundant species) are processed by $\log_2$ transformation and auto-scaling.

Abbreviations: RSV, respiratory syncytial virus; RV, rhinovirus; RV-A, rhinovirus A; RV-C, rhinovirus C

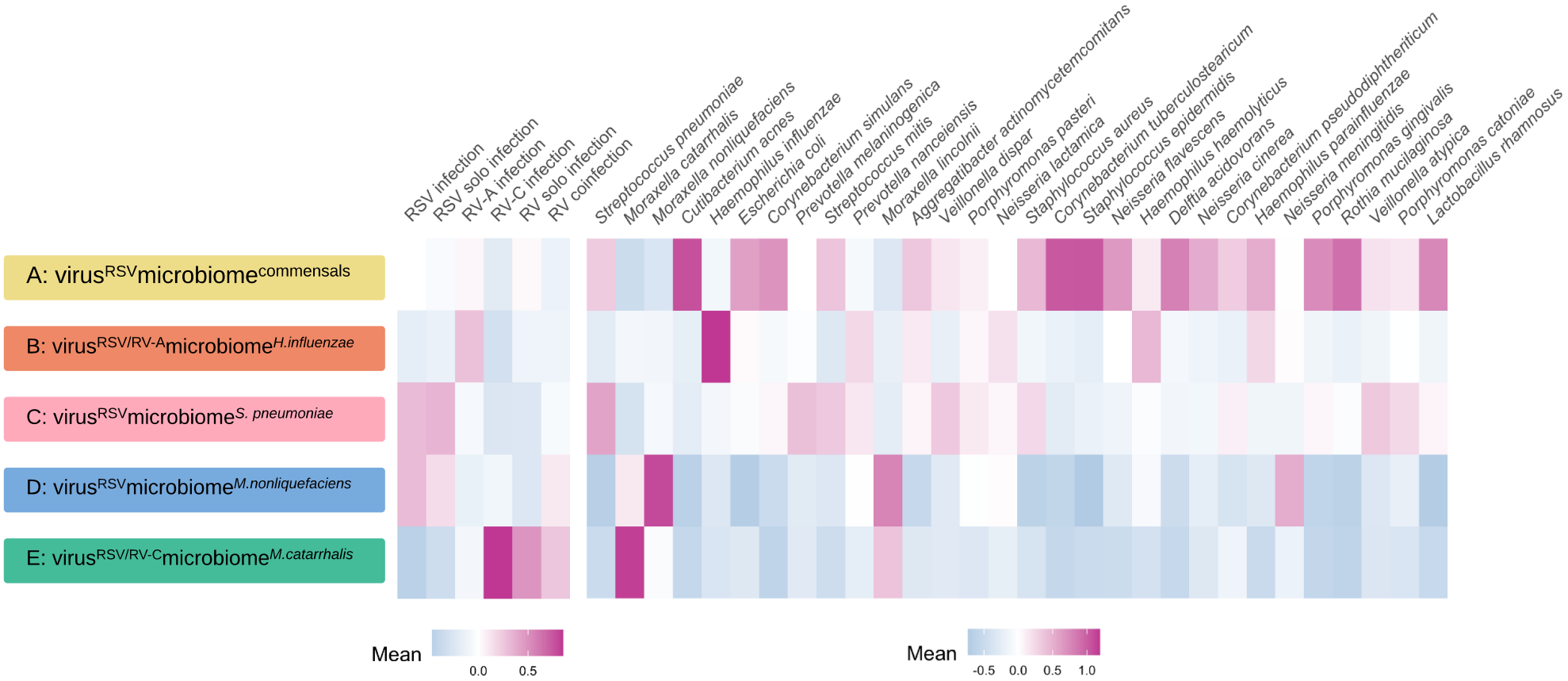

Supplementary Figure S8. Ranking of normalized mutual information score
The ranking of normalized mutual information score of each dataset is shown in the three plots: **A.** virus data; **B.** microbiome taxonomy data (top 20 score species); and **C.** microbiome function data (top 30 score level-2 functions)

Abbreviations: RSV, respiratory syncytial virus; RV-A, rhinovirus A; RV-C, rhinovirus C

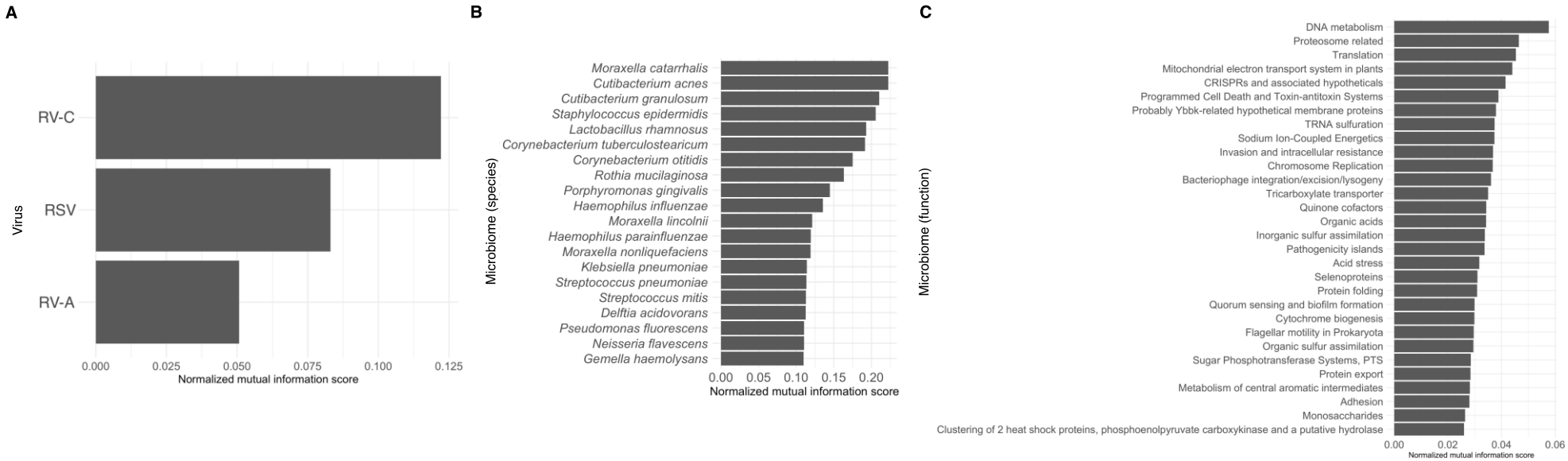

Supplementary Figure S9. Between-profile differences in focused nasopharyngeal microbiome functions in the metatranscriptome profiles A vs. B comparison

The differences in more-detailed microbiome functions (level 3 functions) of the specific level 1 functions (virulence, iron acquisition and metabolism) are visualized. In all comparisons, the mean values of microbiome function variables in the corresponding profiles are plotted. The microbiome function variables are standardized by using auto-scaling after variance stabilizing transformation. Each colour in the microbiome function variables in the Y-axis corresponds to the specific level-2 functions of interest.

A. Profiles A vs. B comparison in virulence (60 level-3 functions)

B. Profiles A vs. B comparison in iron acquisition and metabolism (27 level-3 functions)

* False discovery rate<0.05

Abbreviations: DNA, deoxyribonucleic acid; MAR, multiple antibiotic resistance; MCE, mammalian cell entry genes

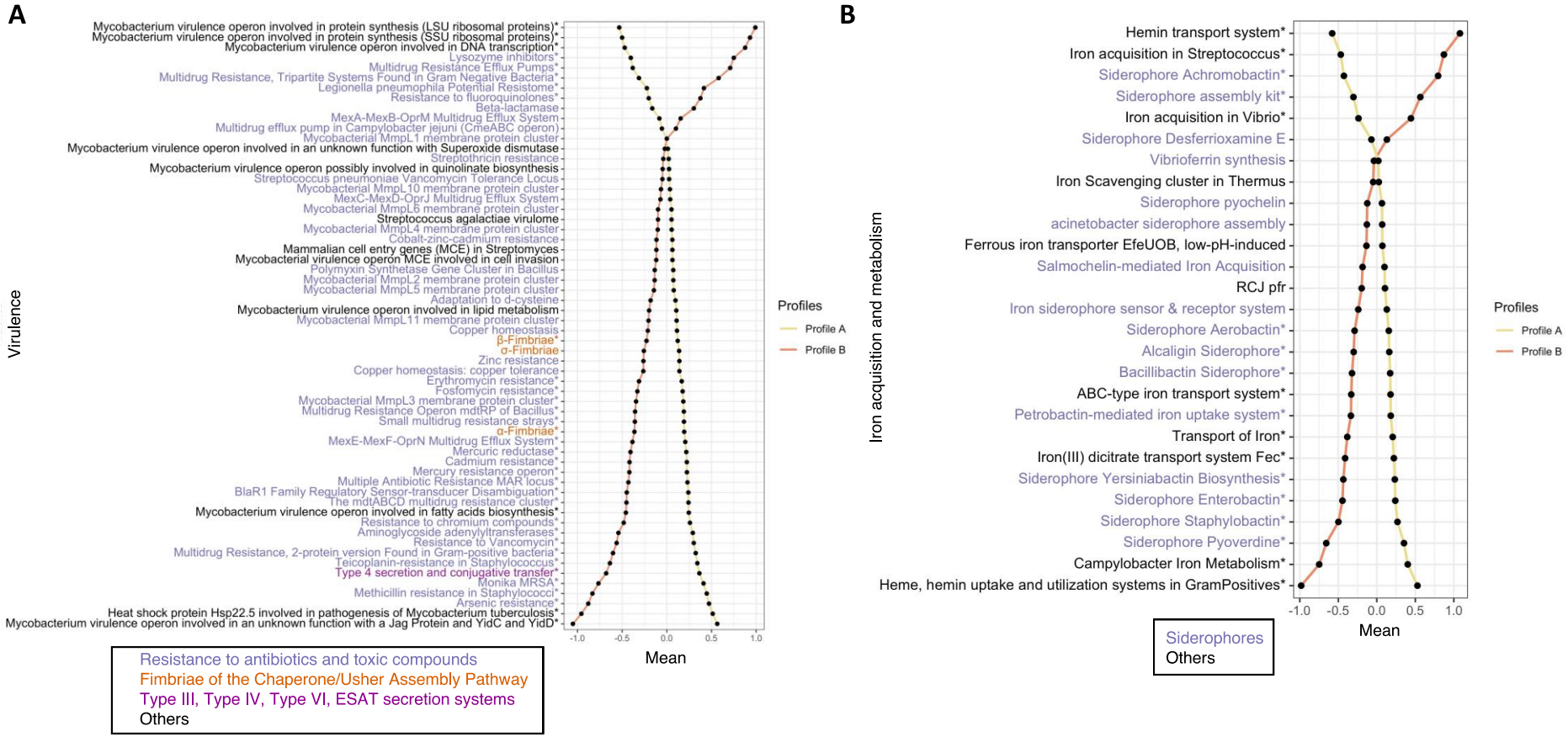

Supplementary Figure S10. Between-profile differences in focused nasopharyngeal microbiome functions in the metatranscriptome profiles A vs. C comparison

The differences in more-detailed microbiome functions (level 3 functions) of the specific level 1 function (the fatty acids, lipids, and isoprenoids metabolism) are visualized. The mean values of microbiome function variables (31 level-3 functions) in the corresponding profiles are plotted. The microbiome function variables are standardized by using auto-scaling after variance stabilizing transformation. Each colour in the microbiome function variables in the Y-axis corresponds to the specific level-2 functions of interest.

* False discovery rate<0.05

Abbreviations: FAS Ⅰ, fatty acid synthase Ⅰ; FAS Ⅱ, fatty acid synthase Ⅱ

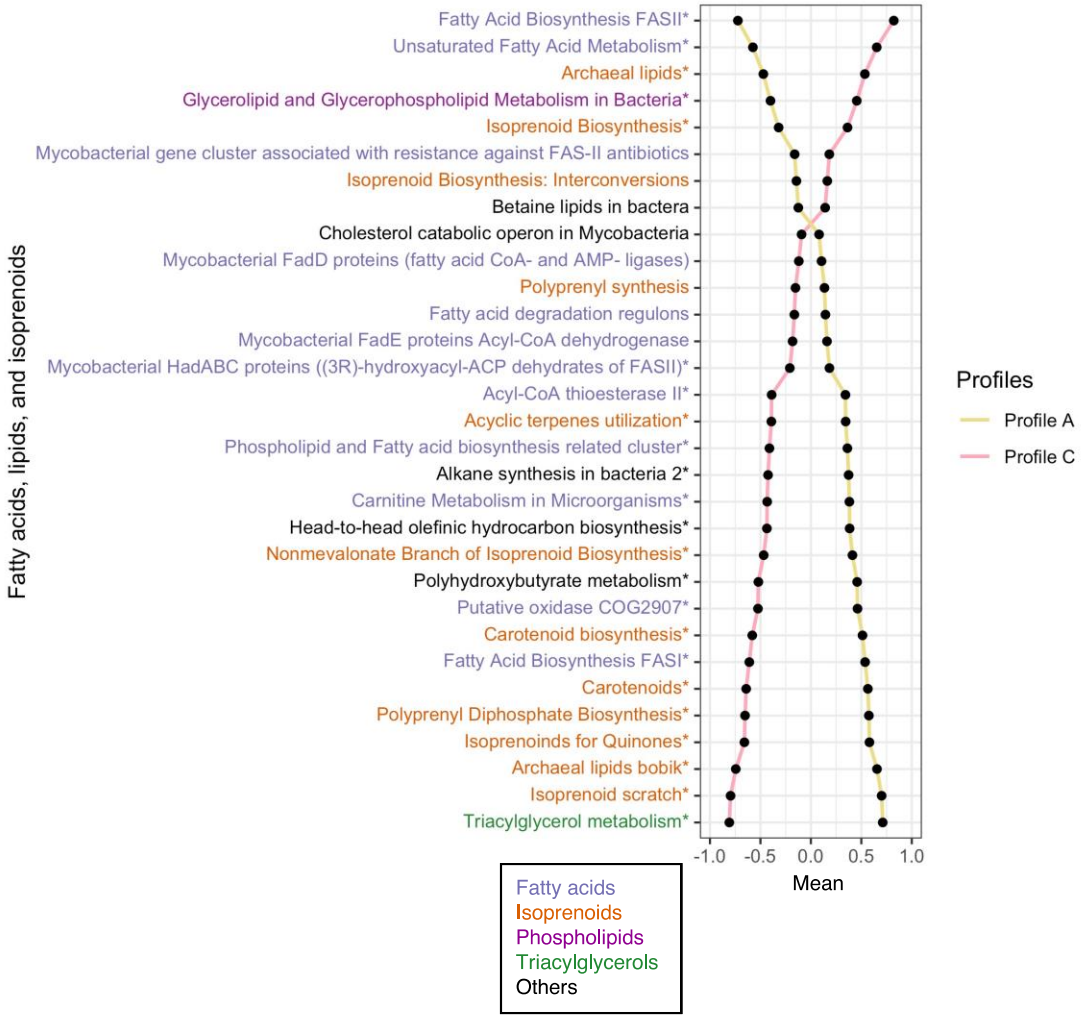

Supplementary Figure S11. Between-profile differences in focused nasopharyngeal microbiome functions in the metatranscriptome profiles A vs. D comparison

The differences in more-detailed microbiome functions (level 3 functions) of the specific level 1 function (the fatty acids, lipids, and isoprenoids metabolism) are visualized. The mean values of microbiome function variables (31 level-3 functions) in the corresponding profiles are plotted. The microbiome function variables are standardized by using auto-scaling after variance stabilizing transformation. Each colour in the microbiome function variables in the Y-axis corresponds to the specific level-2 functions of interest.

* False discovery rate<0.05

Abbreviations: FAS Ⅰ, fatty acid synthase Ⅰ; FAS Ⅱ, fatty acid synthase Ⅱ

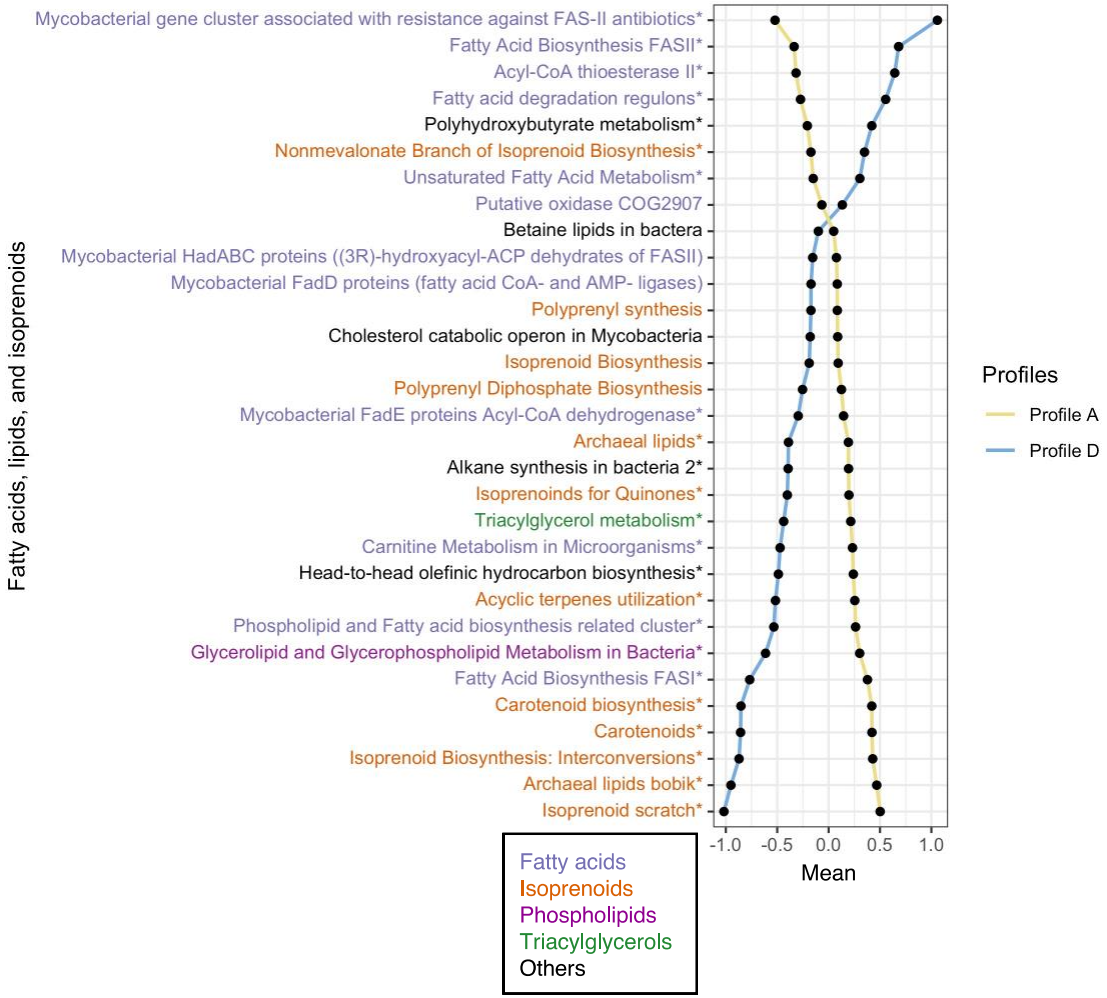

Supplementary Figure S12. Between-profile differences in focused nasopharyngeal microbiome functions in the metatranscriptome profiles A vs. E comparison

The differences in more-detailed microbiome functions (level 3 functions) of the specific level 1 function (stress response) are visualized. The mean values of microbiome function variables (45 level-3 functions) in the corresponding profiles are plotted. The microbiome function variables are standardized by using auto-scaling after variance stabilizing transformation. Each colour in the microbiome function variables in the Y-axis corresponds to the specific level-2 functions of interest.

* False discovery rate<0.05

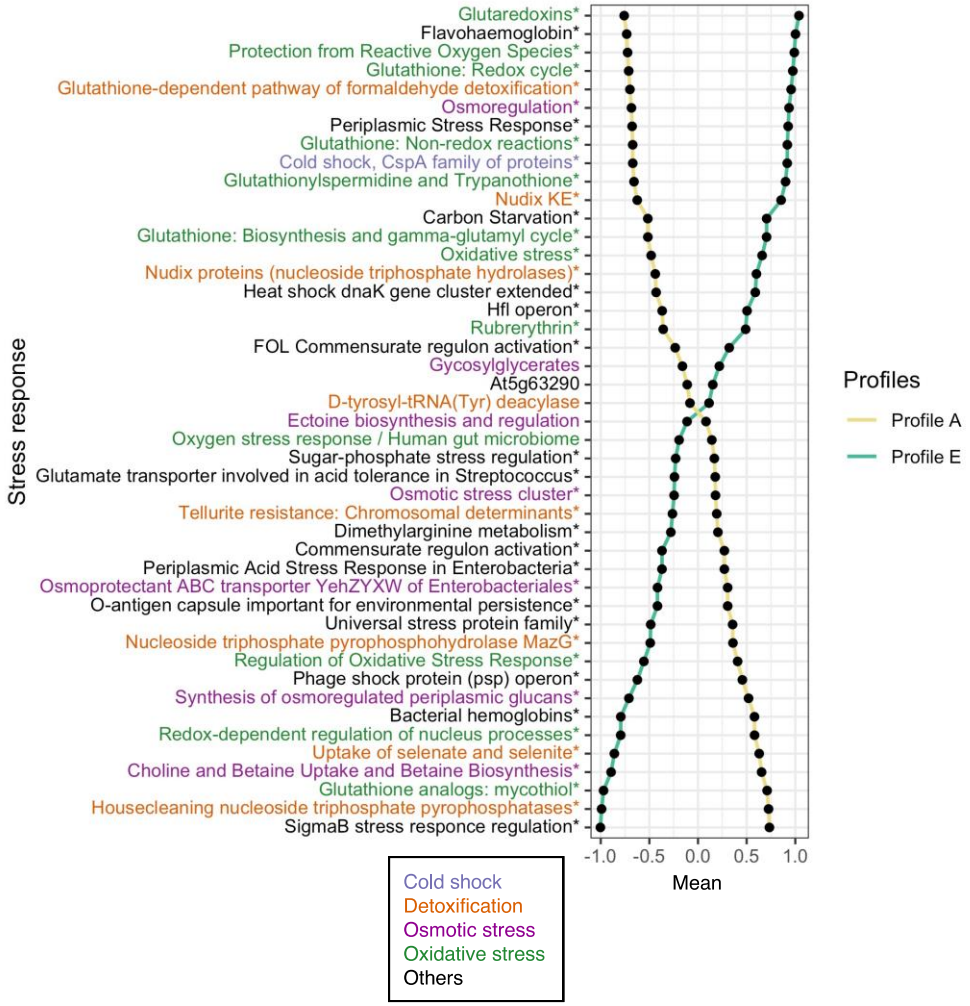

Supplementary Figure S13. Host functional pathway analysis in the metatranscriptome profiles A vs. B comparison
Profile B infants had 63 differentially enriched pathways (FDR<0.05 and percentage of hit genes>70%). For the functional class scoring analysis, we selected 30 pathways with the highest gene ratio to visualize the plot.
Abbreviations: ATP, adenosine triphosphate; DNA, deoxyribonucleic acid; ESCRT, endosomal sorting complexes required for transport; FDR, false discovery rate; GABA, gamma-aminobutyric acid; GABA-A, gamma-aminobutyric acid A; MHC, major histocompatibility complex; mRNA, messenger ribonucleic acid; RAGE, receptor for advanced glycation end products

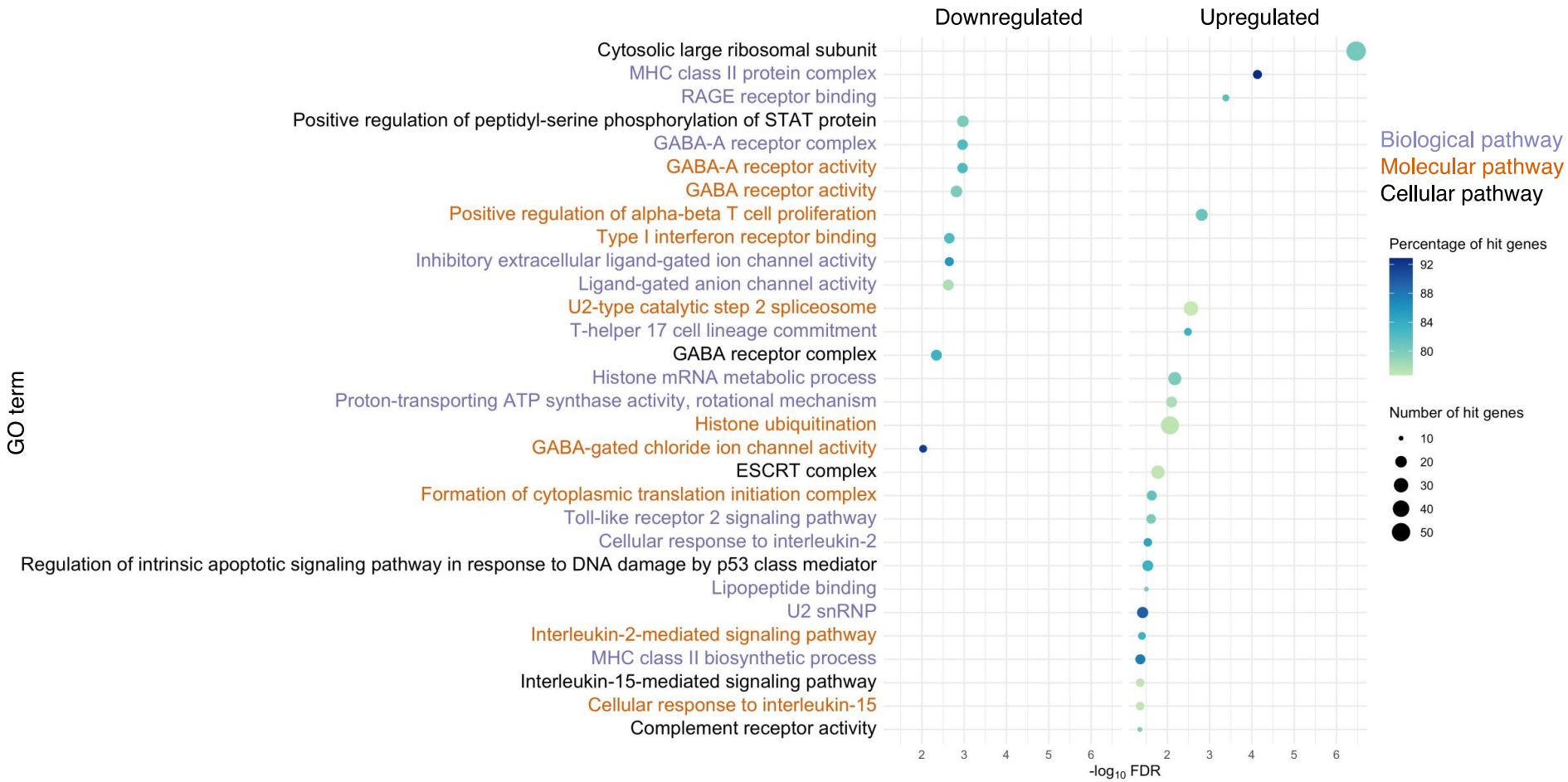

Supplementary Figure S14. Host functional pathway analysis in the metatranscriptome profiles A vs. C comparison
Profile C infants had 45 differentially enriched pathways (FDR<0.05 and percentage of hit genes>70%). For the functional class scoring analysis, we selected 30 pathways with the highest gene ratio to visualize the plot.
Abbreviations: CTD, carboxy-terminal domain, FDR, false discovery rate; GABA, gamma-aminobutyric acid; MHC, major histocompatibility complex; RAGE, receptor for advanced glycation end products; RNA, ribonucleic acid

Supplementary Figure S15. Host functional pathway analysis in the metatranscriptome profiles A vs. D comparison
Profile D infants had 35 differentially enriched pathways (FDR<0.05 and percentage of hit genes>70%). For the functional class scoring analysis, we selected 30 pathways with the highest gene ratio to visualize the plot.
Abbreviations: FDR, false discovery rate; GABA, gamma-aminobutyric acid; GABA-A, gamma-aminobutyric acid A; MHC, major histocompatibility complex; mRNA, messenger ribonucleic acid

Supplementary Figure S16. Host functional pathway analysis in the metatranscriptome profiles A vs. E comparison
Profile E infants had 37 differentially enriched pathways (FDR<0.05 and percentage of hit genes>70%). For the functional class scoring analysis, we selected 30 pathways with the highest gene ratio to visualize the plot.
Abbreviations: ADP, adenosine diphosphate; FDR, false discovery rate; GABA, gamma-aminobutyric acid; GABA-A, gamma-aminobutyric acid A; NAD+, nicotinamide adenine dinucleotide; NAD(P)+, Nicotinamide adenine dinucleotide phosphate

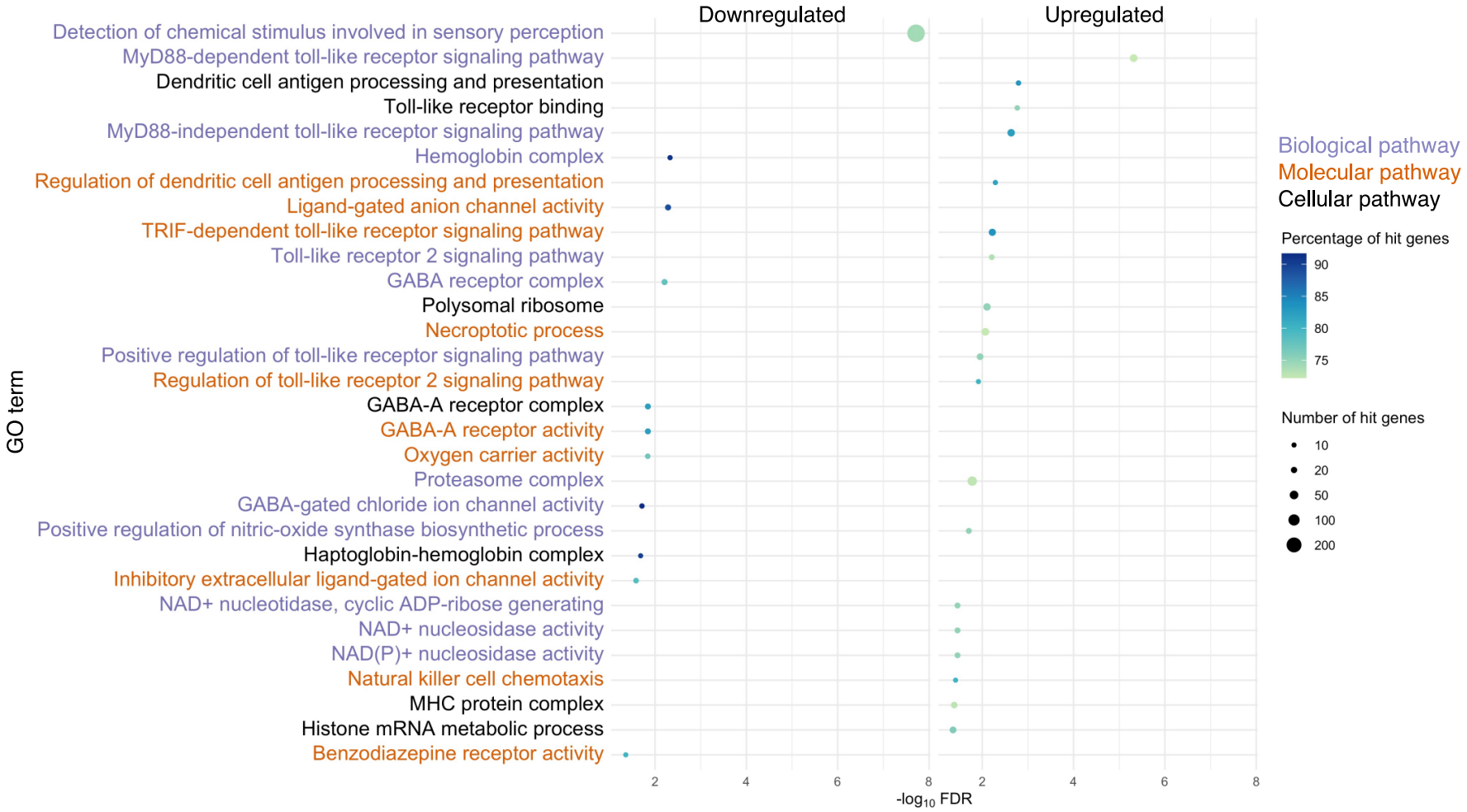

Supplementary Figure S17. Association between nasopharyngeal metatranscriptome profiles of infant bronchiolitis and risk for developing asthma, according to recurrent wheeze status

* Multivariable random-effect logistic model adjusted for age, sex, and clustering within hospitals

Abbreviation: CI, confidence interval; RSV, respiratory syncytial virus; RV, rhinovirus

A. Risk of developing asthma at age 5 years *with* recurrent wheeze by age 3 years (compared to children without asthma or recurrent wheeze)

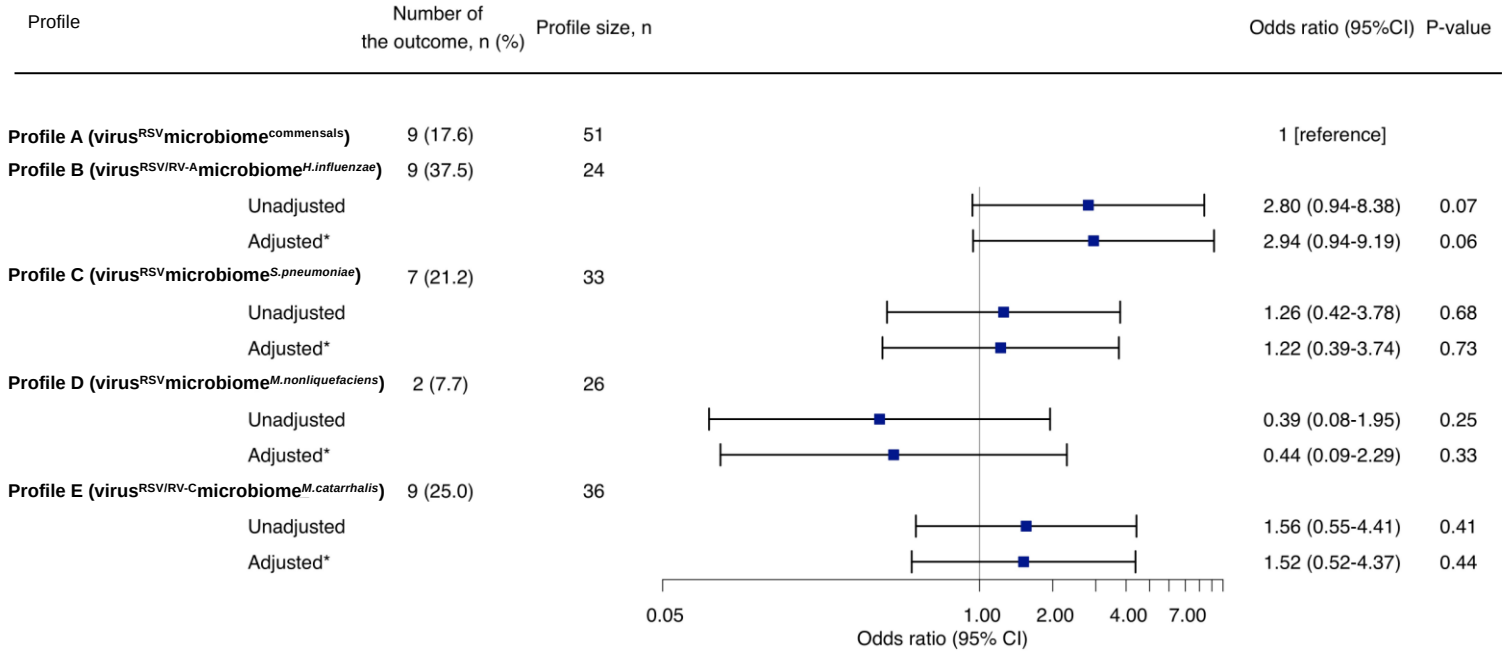

B. Risk of developing asthma at age 5 years *without* recurrent wheeze by age 3 years (compared to children without asthma or recurrent wheeze)

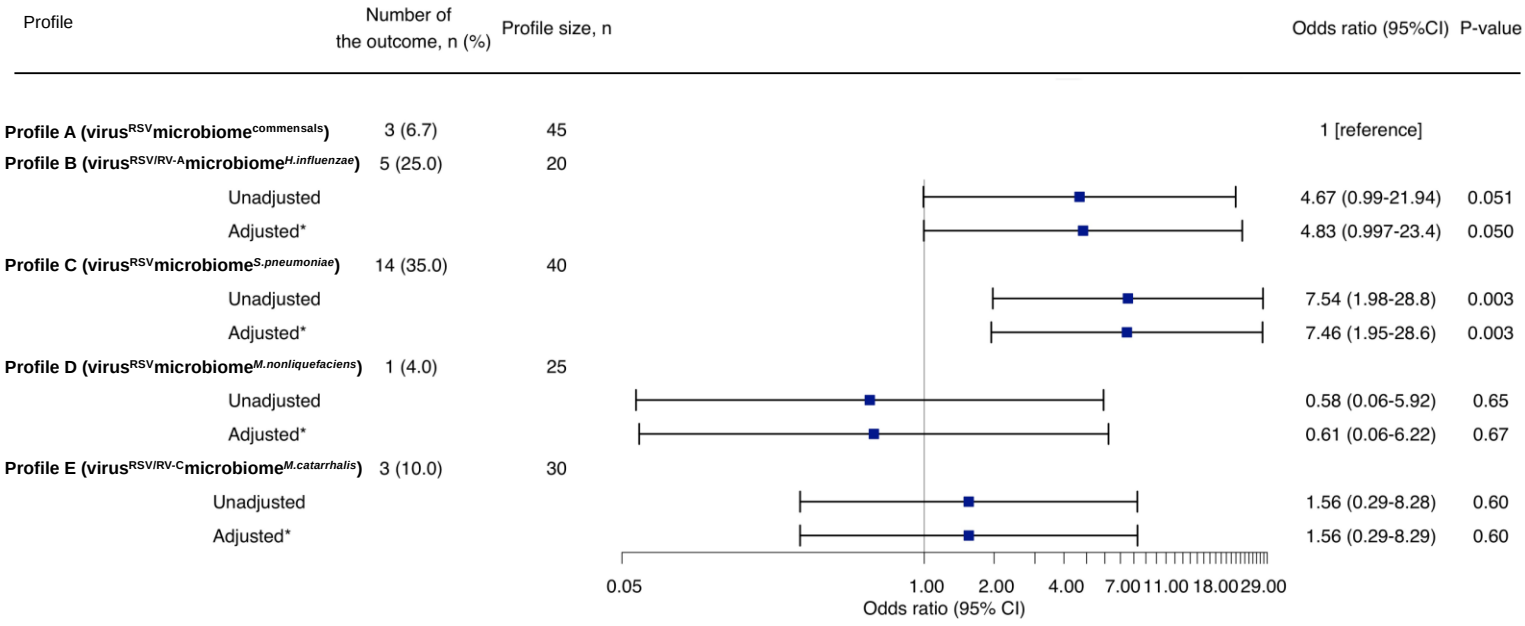

Supplementary Figure S18. Alluvial plot that examines consistencies across different number of profiles

Each color band represents a group of infants with an original profile (A-E). There are consistencies between the five original profiles (A-E) and four and six profiles. The numbers of infants assigned to each profile are presented in **Table E3**.

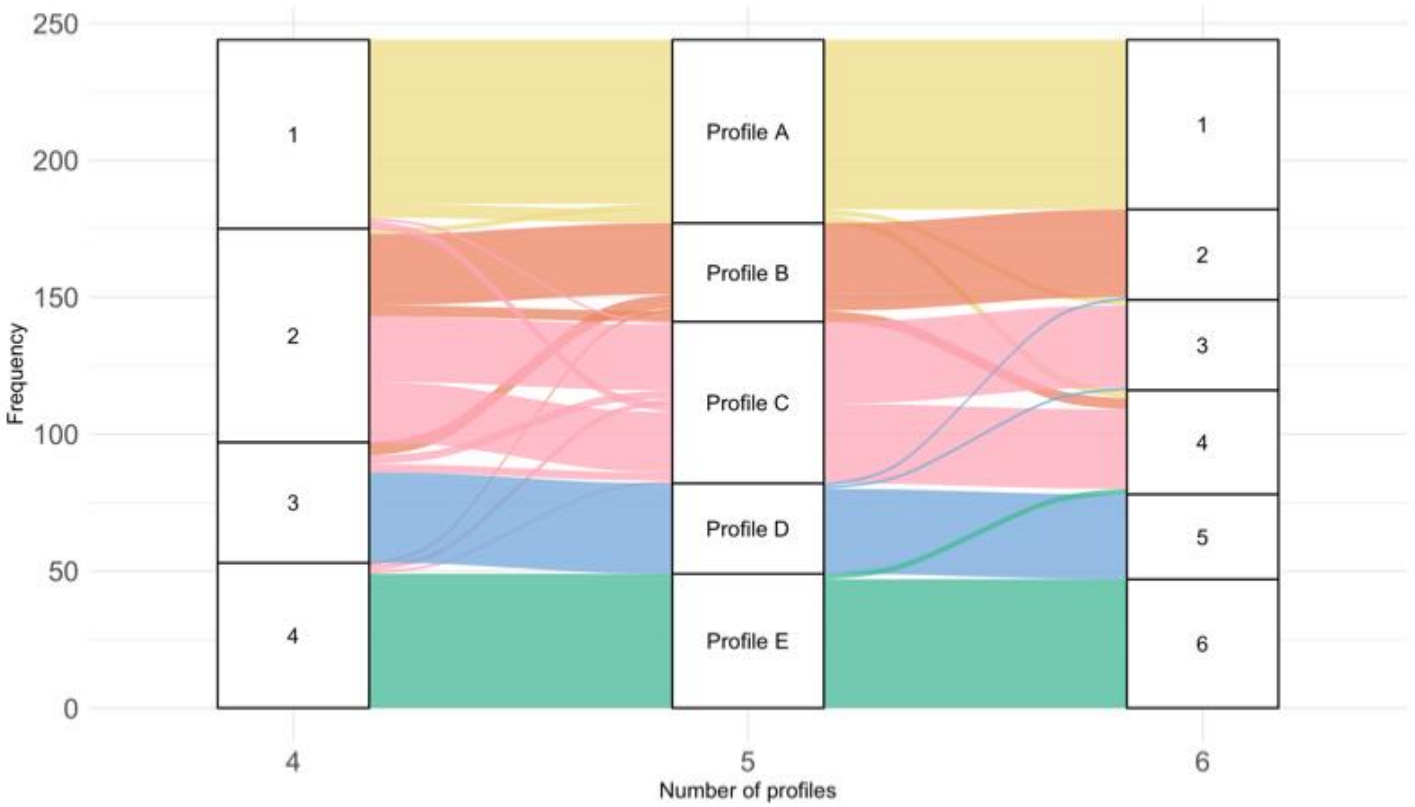

Supplementary Figure S19. Between-profile differences in relative abundance of ten most abundant nasopharyngeal microbial species among infants with bronchiolitis, using four profiles in the sensitivity analysis

The boxplots show the distribution of the ten most abundant species in the nasopharyngeal microbiome, according to the four metatranscriptome profiles. In the overlying violin plots, the width represents the probability that infants in a profile take on a specific relative abundance. The differences in the relative abundance were tested by the Kruskal-Wallis test.

Abbreviation: FDR, false discovery rate

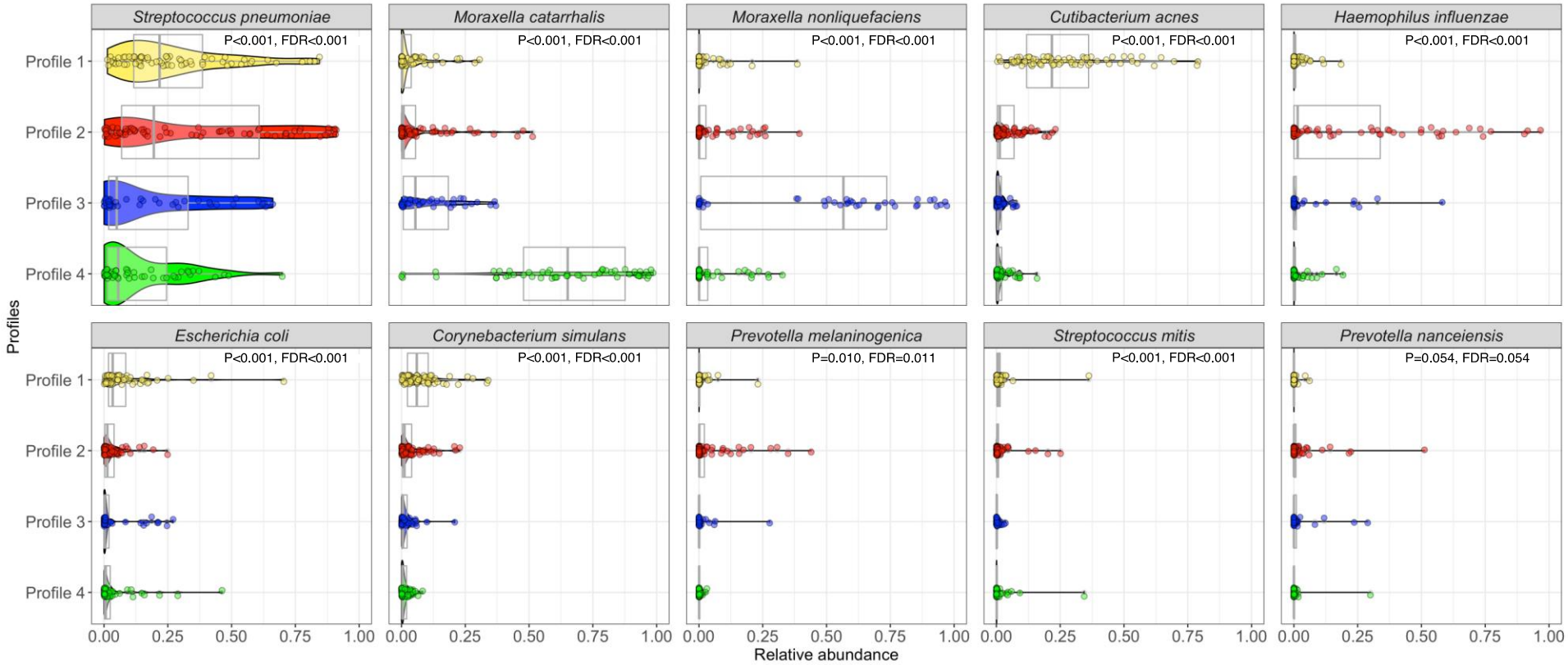

Supplementary Figure S20. Between-profile differences in nasopharyngeal microbiome function in the metatranscriptome profiles 1 (concordant with profile A) vs. 2 (concordant with profiles B and C) comparison, using four profiles in the sensitivity analysis

The mean values of microbiome function variables (35 level-1 functions) in the corresponding profiles are plotted. The microbiome function variables are standardized by using auto-scaling after variance stabilizing transformation.

* False discovery rate <0.05

Abbreviations; DNA, deoxyribonucleic acid; RNA, ribonucleic acid

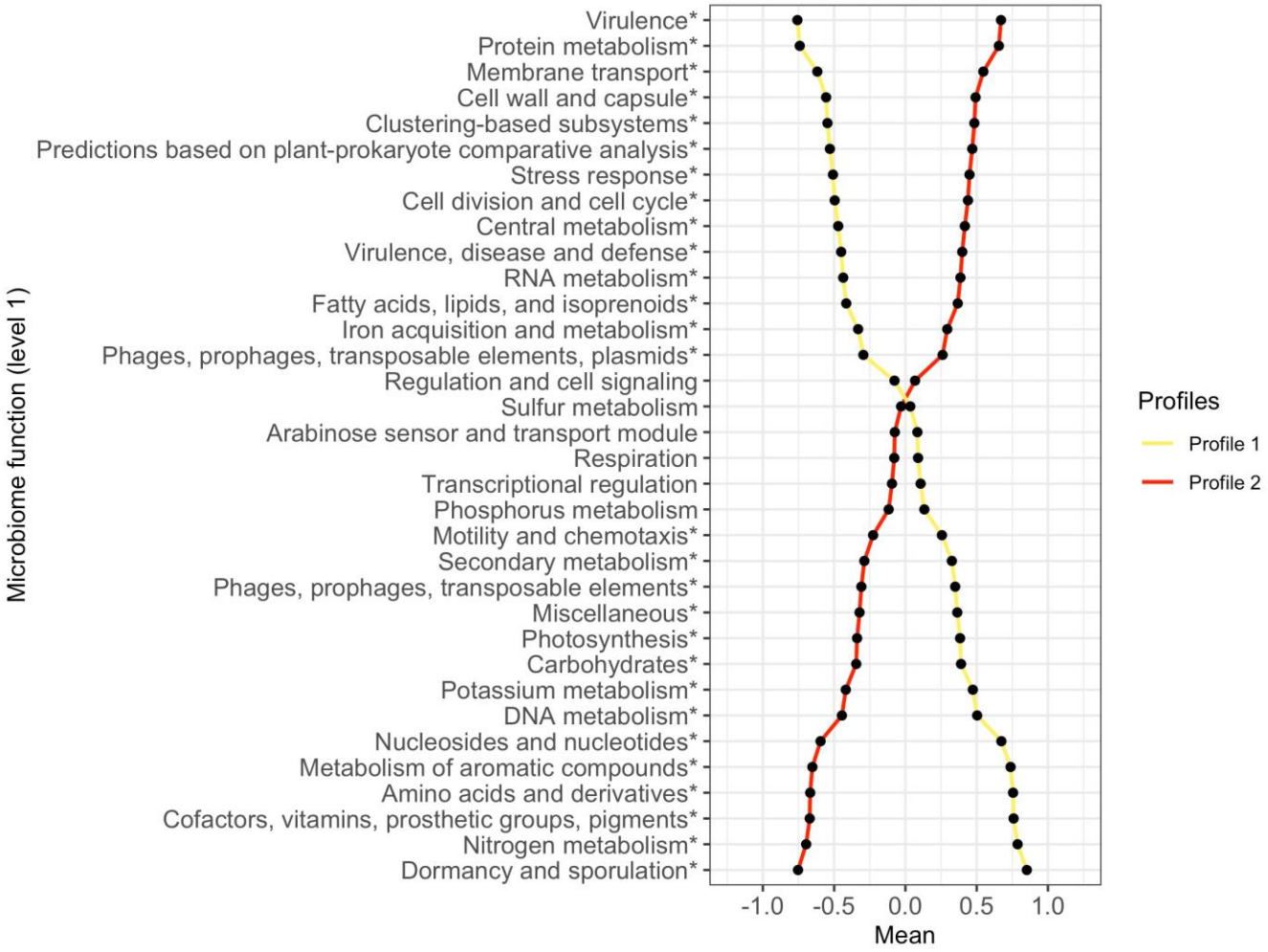

Supplementary Figure S21. Association between nasopharyngeal metatranscriptome profiles of infant bronchiolitis and risk for developing asthma, using four profiles in the sensitivity analysis

Asthma (binary outcome) was defined as physician-diagnosis of asthma at age 5 years, plus either asthma medication use (e.g., albuterol inhaler, inhaled corticosteroids, montelukast) or asthma-related symptoms in the preceding year. To examine the association between bronchiolitis profiles (profile A as the reference) and the risk of developing childhood asthma, logistic regression models were fit.
* Multivariable random-effect logistic model adjusted for age, sex, and clustering within hospitals
Abbreviation: CI, confidence interval; RSV, respiratory syncytial virus; RV, rhinovirus

Profile	Number of the outcome, n (%)	Profile size, n	Odds ratio (95%CI)	P-value
Profile 1 (concordant with profile A)	13 (18.8)	69	1 [reference]	
Profile 2 (concordant with profiles B and C)	27 (34.6)	78		
Unadjusted			2.30 (1.08-5.10)	0.035
Adjusted*			2.25 (1.05-5.00)	0.041
Profile 3 (concordant with profile D)	10 (27.3)	44		
Unadjusted			1.28 (0.49-3.25)	0.61
Adjusted*			1.24 (0.48-3.19)	0.65
Profile 4 (concordant with profile E)	12 (22.6)	53		
Unadjusted			1.29 (0.52-3.18)	0.57
Adjusted*			1.23 (0.50-3.04)	0.65